

KfK 5024
Mai 1993

An Improved Method for Calculating Control Rod Reactivity Worths in Fast Sodium Cooled Reactor Cores

**W. Zwermann, S. Langenbuch, H. Giese, E. Kiefhaber
Institut für Neutronenphysik und Reaktortechnik
Projekt Nukleare Sicherheitsforschung**

Kernforschungszentrum Karlsruhe

KERNFORSCHUNGSZENTRUM KARLSRUHE
Institut für Neutronenphysik und Reaktortechnik
Projekt Nukleare Sicherheitsforschung

KfK 5024

**An Improved Method for Calculating Control Rod Reactivity Worths in
Fast Sodium Cooled Reactor Cores**

W. Zwermann⁺, S. Langenbuch⁺

H. Giese, E. Kiefhaber

⁺ Gesellschaft für Reaktorsicherheit (GRS), Garching

Kernforschungszentrum Karlsruhe GmbH, Karlsruhe

Als Manuskript gedruckt
Für diesen Bericht behalten wir uns alle Rechte vor

Kernforschungszentrum Karlsruhe GmbH
Postfach 3640, 7500 Karlsruhe 1

ISSN 0303-4003

An Improved Method for Calculating Control Rod Reactivity Worths in Fast Sodium Cooled Reactor Cores

ABSTRACT

An improved method is presented to determine the reactivities of strongly inhomogeneous control rod arrangements in fast sodium cooled reactor cores. The method is based on a detailed evaluation of the multiplication constants for the rods embedded in a large surrounding of fuel material. These calculations are performed using two-dimensional transport theory, with an accurate representation of the actual geometry in $R\theta$ coordinates and with fine discretizations in coordinate space and energy. Three-dimensional whole core calculations are carried out in diffusion approximation, with a coarse spatial hexagonal-Z mesh and few energy groups, replacing the individual reactor cells by homogeneous arrangements. The homogenized macroscopic group cross sections are generated with standard methods, however using reduced boron contents of the absorber pins as compared with their actual values. The appropriate boron concentrations are found by comparing the control rod reactivity worths resulting from the two-dimensional transport calculations with those determined from corresponding diffusion calculations with homogenized compositions for the corresponding regions, which possess as many features of the final whole core calculations as possible. In this way, the corrections necessitated by the heterogeneity, transport, mesh, and condensation effects are incorporated in the macroscopic cross sections. With these as input, the computed rod worths of the secondary shutdown system of the SUPERPHENIX-1 (SPX-1) power production core are essentially improved as compared with results of earlier calculations. This progress of the calculational method is clearly demonstrated by a comparison with measured reactivity worths.

Eine verbesserte Methode zur Berechnung von Kontrollstab-Reaktivitätswerten in schnellen natriumgekühlten Reaktorkernen

KURZFASSUNG

Im vorliegenden Bericht wird eine Methode zur Reaktivitätsbestimmung von stark inhomogenen Steuerstabanordnungen in schnellen natriumgekühlten Reaktoren vorgestellt. Die Methode basiert auf einer detaillierten Bestimmung der Multiplikationskonstanten für den Fall, in dem die Stäbe in eine große Zone von Brennstoffmaterial eingebettet sind. Diese Rechnungen werden in zweidimensionaler Transporttheorie durchgeführt, mit einer genauen Nachbildung der tatsächlichen Geometrie in $R\theta$ -Koordinaten und mit feiner Diskretisierung im Ortsraum und in der Energie. Dreidimensionale Ganzkernrechnungen werden in Diffusionsnäherung mit einem groben Hexagonal-Z-Ortsgitter und wenigen Energiegruppen durchgeführt, wobei die einzelnen Reaktorzellen durch homogene Anordnungen ersetzt werden. Die Homogenisierung der makroskopischen Gruppenwirkungsquerschnitte erfolgt mit üblichen Methoden, jedoch wird der Borgehalt der Absorberstäbe gegenüber dem tatsächlichen Wert verringert. Die angepaßten Borkonzentrationen werden durch Vergleich der Steuerstabreaktivitätswerte festgelegt, die sich aus den zweidimensionalen Transportrechnungen ergeben, mit denjenigen aus entsprechenden Diffusionsrechnungen mit homogenisierten Materialmischungen für die entsprechenden Bereiche. Es wird darauf geachtet, daß das dazu verwendete Rechenmodell in möglichst vielen Punkten mit demjenigen der abschließenden Ganzkernrechnungen vergleichbar ist. Dementsprechend sind die Korrekturen, die der Heterogenitäts-, der Transport-, der Maschen- und der Kondensationseffekt erfordern, in den makroskopischen Wirkungsquerschnitten enthalten. Mit diesen Wirkungsquerschnitten als Eingabe verbessern sich die berechneten Stabwerte des Zweitabschaltsystems des SUPERPHENIX-1 (SPX-1)-Leistungskerns wesentlich gegenüber den Ergebnissen früherer Rechnungen. Dies wird durch einen Vergleich mit gemessenen Reaktivitäten bestätigt.

1.	INTRODUCTION	1
2.	SURVEY OF THE FORMER AND PRESENT APPROACHES TO PRODUCE HOMOGENIZED ABSORBER CROSS SECTIONS	4
3.	DETAILS OF THE PRESENT CALCULATIONS FOR THE BARE CONTROL RODS	7
3.1	The Reference Calculations	7
3.1.1	The Control Rod and Sodium Follower Models	7
3.1.2	Reference Transport Model Calculations and Results	8
3.1.3	Confirmation of the Results	11
3.2	Homogenization of the Control Rods	14
3.2.1	Calculation of First Estimate Homogenous Cross Sections	15
3.2.2	Adjustment of the Homogenous Cross Sections	16
4.	RESULTS OF THE WHOLE CORE DIFFUSION CALCULATIONS FOR SPX-1	20
5.	CRITICAL REMARKS ON THE USED BUCKLING	22
6.	SUMMARY AND OUTLOOK	26
	References	33
	Appendix: List of Used Numerical Programmes	37
	Tables	39
	Figures	48

1 INTRODUCTION

In order to guarantee the shut-down safety of a nuclear power reactor, it is necessary to determine the reactivity changes caused by the movement of control rods with high accuracy. Therefore, it would be desirable to perform calculations on the highest level of computational methods available, i.e. using transport theory with high resolution in space and energy variables, and to describe the geometry of the arrangement very precisely. However, for the entire fuel zone of a nuclear power plant, this task is far from being practicable up to now due to restrictions on CPU time and storage capacity even with the most powerful computers, since the reactor core is a very complex heterogeneous geometrical arrangement, consisting of some hundreds of elements of different kinds (fuel elements, control rods, etc.), which, on their parts, in general possess a pronounced internal structure. Hence, a number of approximations have to be applied. In order to make the problem tractable, the diffusion approximation to the transport equation is applied, with a relatively coarse spatial resolution to limit the number of mesh points. To make this coarse mesh calculations possible, the internal structure of the individual elements cannot be described anymore; rather, the actual element geometries and material compositions are replaced by appropriate homogeneous arrangements. In addition, to keep computational cost and storage requirements acceptable, it is advisable to restrict the calculations to a small number of energy groups.

The main task consists in producing appropriate homogeneous macroscopic cross sections for the various elements of the reactor core, which make the corresponding material mixtures neutronically equivalent to the original heterogeneous arrangements. This type of adapted homogenization procedure for the secondary shut-down system SAC (système d'arrêt complémentaire) of the French fast sodium cooled reactor SUPERPHENIX-1 (SPX-1) /1/, is the subject of the present investigation.

Diffusion calculations for the SPX-1 core have already been performed earlier by BELGONUCLÉAIRE (BN) and Kernforschungszentrum Karlsruhe (KfK) /2/. The set of homogeneous macroscopic cross sections for the various hexagonal cells of the reactor core needed as input was generated from simplified one-dimensional cylindrical models of the cells. The heterogeneous cross sections were flux-volume weighted with the help of the results of corresponding collision probability calculations for these models.

This analysis resulted in rod worths for the secondary shut-down system of SPX-1 which were too large by approximately 20 % as compared with the corresponding experimental values. An overestimation of this magnitude was rather surprising, since similar calculations for the critical assemblies SNEAK, ZEBRA and MASURCA had yielded substantially smaller deviations from the experimental rod worths /2,3/. It has to be noticed, however, that the SPX-1 control rods exhibit a much more pronounced degree of heterogeneity than those of the corresponding control rod designs investigated in most of the critical experiments. A secondary shut-down system rod is schematically shown in Fig. 1; it consists of three vertical active sections, the upper and middle of which are identical. (We shall from now on use the notations "lower SAC" and "upper SAC" for the lower part of the control rod, and for the upper and middle parts, respectively).

It can be seen from Fig. 1 that a one-dimensional cylindrical modelling of the SACs can be performed only in a very schematical way, which makes the homogenization procedure based on this modelling more doubtful than in cases where the absorber arrangements are less heterogeneous. Furthermore, in establishing the one-dimensional model an appreciable degree of arbitrariness is introduced in quantities which are important for the neutron flux distributions, like the surface-to-volume ratio of the absorber material; this deteriorates the reliability of the final whole-core results.

Although there exist various refined methods for generating homogeneous cross sections based on one-dimensional control rod models /4-8/, these procedures are sometimes fairly complicated and in general suffer more or less from the shortcomings implied by the simplified representation of the absorber geometry. In the present investigation, a method is presented which is based on a two-dimensional reference transport calculation with a rather detailed modelling of the control rod geometry. Although the absorber cross sections are again homogenized using a one-dimensional cylindrical model, the disadvantages arising from this procedure are substantially mitigated. This is achieved because not the primary homogeneous cross sections resulting from the one-dimensional transport runs are taken as input to the whole-core diffusion calculation; rather, these cross sections are adjusted on the basis of the desired reference rod worths.

After briefly outlining the earlier KfK/BN method, the new concept is described in section 2, and the essential differences between both strategies are explained. Details of

the calculations for the absorber elements are presented in section 3. First, we give a description of the reference transport calculations, including the geometrical model for the control rods, and then address the production of modified homogenized cross sections. In section 4, results of whole-core diffusion calculations using these cross sections as input for the secondary shut-down system are presented. After some critical remarks concerning the used buckling (section 5), we close the presentation with a brief summary and give our conclusions in section 6. An overview of the applied numerical programmes can be found in the appendix.

As this work was performed in cooperation between GRS and KfK, it will be published as GRS-report and in the same form as KfK-report.

2 SURVEY OF THE FORMER AND PRESENT APPROACHES TO PRODUCE HOMOGENIZED ABSORBER CROSS SECTIONS

Before presenting our method for computing the SAC-reactivities in detail, we briefly review the strategy used so far by KfK/BN.

For both parts of the SAC, homogenized cross sections were generated with the one-dimensional collision probability code KAPER4 /9/. To apply this method, the actual absorber pins had to be replaced by azimuthally homogeneous structures, namely a ring for the lower and a cylinder for the upper SAC, both containing mixtures of boron carbide, sodium and steel, such that the original material amounts were preserved, with outer (and for the ring also inner) radii equalling the radii of the pin envelopes, cf. Fig. 2. These arrangements were embedded in a fuel ring of 20 cm thickness. The neutron fluxes were determined for 26 energy groups, with the KFKINR nuclear data library /10/ as basis. Using the results of the "old supercell model" calculations, so-called transport corrected homogeneous cross sections were generated by a flux-volume weighting over the control rod region. These cross sections were finally collapsed to four energy groups and used as input for the SAC regions in whole core calculations in three-dimensional coarse mesh hexagonal geometry with the finite difference diffusion code D3D/D3E /11/. Obviously, by this method, uncertainties are introduced, whose effects on the final results are difficult to estimate a priori, mainly arising from the rough geometrical model used for the homogenization procedure, and from shortcomings of the diffusion approximation employed for the control rod worth calculations. In Table 1, computed SAC rod worths /2/ are shown for two different insertion depths of the main control system SCP (système de commande principal), and compared with values measured in the start-up phase. The unit pcm means that the reactivities $(k-1)/k$, where k is the multiplication constant, as well as differences between them, are multiplied by 10^5 . It can be seen that the experimental results were strongly overestimated.

To get rid of at least part of the difficulties involved in the method outlined above, a new approach for obtaining appropriate homogenized cross sections is chosen, which is described in the following.

As a first step, the reactivity worths of the bare SAC segments, i.e. embedded in a large homogeneous core cylinder, are computed against a sodium follower in the best

way that is possible. For this purpose, the two-dimensional transport code TWODANT /12/ in R θ geometry is employed. These "reference transport model" calculations are performed for detailed representations of the real absorber geometries with high space and energy resolution.

In the next step, homogenized cross sections are produced in a similar manner as with the old supercell model, namely for one-dimensional arrangements with the KAPER4 code. But in contrast to the former approach, these cross sections are now to be considered only as a first guess and will be modified iteratively in an appropriate way.

With these cross sections, diffusion calculations are performed to obtain the reactivity differences between the sodium follower and the homogenized bare control rods, again embedded in a core cylinder as it was the case in the transport calculations. The D3D/D3E code is run in cylindrical geometry mode with the input chosen as similar to the final whole core calculations as possible, namely in three dimensions, with a coarse spatial mesh and few energy groups. As could be expected, the reactivity differences obtained within these homogeneous calculations do not agree with the reference values from the TWODANT calculations; they are too large in absolute magnitude, i.e., the homogenized control rod models in diffusion approximation are too effective as compared with the detailed ones in transport theory.

To remedy this deficiency, the homogeneous cross sections have to be altered such that the absorption effect is reduced. This is done by performing again KAPER4 calculations with suitably modified input data to be described later in detail. With these new cross sections, the new reactivity worths obtained in subsequent diffusion calculations are already closer to the reference values.

The remainder of the procedure is rather straightforward: alternately KAPER4 and D3D/D3E are run to produce modified homogeneous cross sections and to calculate reactivity differences with these as input, respectively, until the transport theory reference values are reproduced. Only few iteration steps are necessary since the reactivity worths from the first few runs can be employed to estimate the correct input parameters for KAPER4. These suitably adjusted cross sections yielding reactivity differences identical to those of the detailed transport calculations are finally used as input for the SAC cells in the whole core diffusion calculations.

In the procedure described above, the reference calculations are performed on a high computational level, whereas the calculations for the corresponding homogeneous arrangements closely resemble the final whole core runs. For that reason, a large part of the corrections necessitated by the rather rough modelling inherent to the whole core calculations are already taken into account in the homogenized cross sections, namely: (1) heterogeneity effects, (2) transport effects, (3) condensation effects, and (4) mesh effects. Hence it can be expected that these cross sections are suitable to describe the SAC cells in the production calculations, so that no a posteriori correction is needed anymore for the resulting control rod worths.

3 DETAILS OF THE PRESENT CALCULATIONS FOR THE BARE CONTROL RODS

In this section, we give a detailed description of our calculations. We begin with the method for obtaining the reference reactivities, and then present the procedure for computing equivalent homogeneous cross sections.

3.1 The Reference Calculations

We attempt to calculate the reactivities of the lower and upper parts of the SAC, embedded in a large cylinder of core material, as exactly as possible with a reasonable amount of computing time. For this purpose, we utilize the two-dimensional transport code TWODANT /12/, which solves the multigroup, time-independent Boltzmann equation with the discrete-ordinates method for the angular dependence of the neutron flux, and the diamond-difference scheme for spatial discretization. As a first step, we have to model the real SAC geometry in a way which is suitable as input for TWODANT.

3.1.1 The Control Rod and Sodium Follower Models

Horizontal cuts through the lower and upper SAC were displayed in Fig. 1a. Among the three geometries possible within TWODANT, XY, RZ, and R θ , the latter one is most appropriate for describing these horizontal cuts. In Fig. 3a, sketches of our models for both parts of the control rod are shown. We have replaced the original hexagonal outer shape by a circle of the same area; the thickness of the steel ring is chosen such that the area of the hexagonal sheath is preserved. The radial midpoints of the model absorber "pins" agree with the centres of the original ones, and the half opening angle ϑ is determined by requiring that the distance between the "pin" radial midpoint and the centre of a side equals the original pin radius r , i.e., $2 R \sin (\vartheta/2) = r$, where R is the distance between the centre of a pin and the rod axis. Furthermore, we require the areas of the model and real absorbers to be identical, yielding for the model "pin" thickness $d = \pi r^2/(2 \vartheta R)$. The model absorber composition is a mixture of the original absorber and steel cladding materials, appropriately diluted to take account of the gap between the absorber cylinder and the cladding. For clarity, a de-

tailed sketch of the upper SAC model geometry is displayed in Fig. 3b. Finally, the arrangements are surrounded by a large fuel annulus of about 120 cm outer radius with vacuum outer boundary condition (cf. Fig. 3); this value for the radius is rather arbitrary and was chosen such that the resulting multiplication constants k_{eff} will not deviate too much from unity.

The model for the follower is obtained by simply substituting each absorber pin with sodium.

After these preparations, the TWODANT input data set for computing the SAC rod worth within the reference transport model can be set up.

3.1.2 Reference Transport Model Calculations and Results

Neutron fluxes and multiplication constants are computed separately for the lower and upper SAC models shown in Fig. 3a, with 26 energy groups on the basis of the KFKINR adjusted nuclear data library, from which macroscopic cross sections are produced with the module GRUCAL /13/ of the KfK programme system KAPROS /14,15/. A fine spatial mesh is applied, with radial widths of about 0.5 cm inside the rod and 2.5 cm inside the fuel annulus, and azimuthal widths of about 3.5° , corresponding to approximately 0.5 cm on the rod surface. For the angular discretization, the S_n order of 4 is chosen. Since $R\theta$ geometry is used, the finite height cannot be described by a z -dependence; therefore, axial leakage must be taken into account in another way. This is done via introducing a material and energy independent buckling by modifying the cross sections applying the KAPROS-module SIGMUT /16/. A numerical value of $B^2 = 8.62 \times 10^{-4} \text{ cm}^{-2}$ is chosen which approximately corresponds to the actual core height of 100 cm; it has been determined by requiring that a three-dimensional D3D/D3E diffusion calculation in $R\theta Z$ geometry with vanishing extrapolated flux as boundary condition and a corresponding $R\theta$ calculation with buckling yield identical multiplication constants for the sodium follower, again placed in a fuel annulus of about 120 cm outer radius, using homogenized KAPER4 cross sections. Provided that the application of a material- and energy-independent buckling is adequate, this value is furthermore confirmed by performing calculations for corresponding ring-shaped control rod models in RZ geometry with the two-dimensional diffusion code DIXY2

(again with vanishing extrapolated flux on the surface) and the related evaluation codes /17/, which allow to calculate bucklings directly.

In Table 2, the main results of our reference calculations are shown, namely the multiplication constants of the sodium follower and both SACs, together with the rod worths.

In Fig. 4, we additionally display contour plots of the neutron fluxes resulting from the reference transport model for one quadrant of the interior section of the lower SAC. For the sake of lucidity, however, these plots refer to a calculation with only four energy groups, where the original 26 groups have been collapsed by using the KAPROS module SIGMNC /18/ according to the scheme 1-4 -> 1; 5,6 -> 2; 7-10 -> 3; 11-26 -> 4. The normalization of the fluxes is chosen such that the fission source rate is normalized to the multiplication constant. (Note that the slight deviations from a symmetrical distribution which are in contradiction to the symmetrical geometry of the SAC absorbers are caused by numerical uncertainties in the data preparation routine for the graphics programme). The graphs illustrate the strong spatial dependence of the neutron fluxes in the region between the absorbers, with large depressions at the positions of the boron carbide pins. This can also be seen in Fig. 5, where the radial dependence of the fluxes is displayed inside the rod at the azimuthal angles of 0° (through the centre of a pin) and 22.5° (between two pins). The vertical lines represent the inner and outer edges of the absorber pins.

Figure 5 also shows the results of a corresponding D3D/D3E diffusion calculation. The fluxes are normalized in the same way as in the transport calculations, i.e. the fission source rate is normalized to k-eff. We recognize that diffusion theory cannot adequately describe the extremely inhomogeneous arrangements we are dealing with; in particular, the flux variation in the absorber region for the high-energy groups is poorly reproduced. As a further illustration for the necessity of a transport calculation, the reactivities resulting from the four-group TWODANT and D3D/D3E runs are compared in Table 3. It should be mentioned that despite the appreciable discrepancies between the 4-group and 26-group multiplication constants computed with transport theory, the rod worths against the sodium follower agree within 10 - 15 pcm, which is less than 1% of the rod worths for both the lower and the upper SAC.

To facilitate the interpretation of the results shown in Figs. 4 and 5, some additional comments might be helpful:

- a) Obviously there is a considerable azimuthal dependence of the neutron fluxes in the radial range 3.5 through 6 cm, i.e., in the region which contains the absorber pins. This effect is not at all surprising but one should have in mind that with the cylindrical model employed in the cross section production of the former analysis, such an effect could not be taken into account.
- b) The azimuthal dependence, i.e., the deviation between the curves for 0° and 22.5° , respectively, is much more pronounced in transport than in diffusion theory.
- c) The flux depression (or the neutron attenuation when going from the fuel region into the absorber region and then towards the centre of the control rod) is stronger in transport than in diffusion calculations (incidentally for group 4 the fluxes in the central part are roughly in agreement). For the proper interpretation of the results presented in Fig. 5 one should have in mind that the ordinate scales are adapted to the respective curves shown for each energy group.
- d) The fluctuations exhibited by the transport solutions inside the homogeneous region within a radius smaller than about 3.5 cm are probably not realistic.

In Fig. 6, the reference transport model results, again computed with only four energy groups, for the sodium follower and both SACs in the whole calculated region, are compared with each other, displaying the global influence of the presence of the absorber elements. Here, the vertical lines denote the edge of the control rods, i. e. the location of the steel sheath.

From the point of view of reactor physics it is interesting to note the remarkable flux peaking in the follower region for the low energy neutrons which are collapsed in group 4 (for the fairly coarse energy group structure used here for illustration purposes).

3.1.3 Confirmation of the Results

After having obtained the reference values for the rod worths in transport theory, we briefly investigate the quality of our calculations with regard to the geometrical model, the spatial grid, and the S_n order.

a) Geometrical Model

In addition to the geometries shown in Fig. 3a, we have also performed 26-group TWODANT calculations with a more detailed description of the absorber pins as outlined in Fig. 7. The results, not only for the reactivity differences, but also for the absolute magnitudes of the multiplication constants, are practically identical to the numbers given in Table 2, with differences in $\Delta k/k$ of less than 2×10^{-5} (less than 0.15 % of the rod worths) for both the lower and the upper SACs.

The neutron fluxes are also fairly similar for both cases, as can be seen by comparing the contour plots resulting from both geometries of the lower SAC in a four energy group calculation, Figs. 4 and 8, with the difference that the edged absorber shapes of the first model were still visible in the flux maps, whereas the fluxes resulting from the detailed geometry representation follow more closely the actually cylindrical shapes of the absorber pins. But in general the shape of the contour lines for corresponding flux levels is in good agreement between Figs. 4 and 8; even the flux level of the minimum and its position within the rod for all energy groups do not differ appreciably between the results for the two models. Only at the lower flux levels close to the centre of the pins some deviations in the shapes can be observed. This confirms that the assumptions inherent in the modelling prescription were reasonable. In particular it was appropriate to keep the absorber area constant because even for the thick SAC pins volume absorption is much more important than surface absorption.

From this satisfactory overall agreement of the results, in particular for the multiplication constants, we conclude that the prescriptions leading to the geometrical model displayed in Fig. 3a are reasonable and may also be used for similar arrangements in future investigations.

At this place, one remark is appropriate concerning the choice of the core radius, which is, within certain limits, a free parameter. It turns out that a variation of this

radius alters not only the multiplication constants, but also the reactivity differences between sodium follower and SACs substantially. (Changing the core radius means that the reactivity worths of both the central follower and the central absorber regions will undergo changes, but not by the same amount). However, this does not influence the homogenized macroscopic cross sections whose generation is described in subsection 3.2, provided that the core radius in the homogeneous diffusion calculations equals that of the transport calculations, since then the corresponding reactivity differences change by the same amount.

b) Spatial Grid

To examine whether the mesh widths chosen are sufficient to produce reliable results, we have calculated multiplication constants with twice the number of meshes in both the radial and azimuthal directions, for four energy groups, however. The differences to the four-group results with the original grid are again negligible, being of the order of 10^{-5} in $\Delta k/k$ for the sodium follower, and even less for the SACs, leading to ~ 0.1 % for the rod worths.

c) S_n Order

Finally, we have increased the S_n order to $n = 8$ and performed the corresponding four-group calculations. Although for this case the discrepancies between the $n = 4$ and $n = 8$ multiplication constants rose to $3 - 6 \times 10^{-4}$, the rod worths differ only by 20 - 30 pcm (i.e., ~ 1.5 % rel.), a magnitude which does not significantly influence our results for the whole core calculations, as will become evident later.

Before closing this section a few remarks seem appropriate.

The R Θ calculational model described above (Fig. 3) allows radial "streaming" of neutrons through the gaps located between the absorber parts. These gaps are filled with coolant which is fairly transparent for neutrons. Thus, this R Θ model fairly well simulates the important flight paths for neutron propagation from the surface to the centre and to the opposite surface of the rod in the real arrangement of absorber pins in the SAC rod.

In addition, the volume (or in this case the area) of the absorber pins is preserved. This type of preservation is an adequate requirement for a fast reactor because the flux depression within the absorber is not too pronounced, as can be seen from Figs. 4 and 8. Thus, volume absorption is more important than surface absorption, which in turn would probably be dominant in thermal reactors for which preservation of the surface instead of the volume (or area) would be a more suitable requirement.

For these reasons, our reference transport model appears reasonable to establish a rather close correspondence between reality and the related calculational model in $R\theta$ -geometry.

When comparing the contour lines in Figs. 4 and 8, respectively, one becomes aware that at levels close to the centre of the pin the lines for the detailed model (Fig. 8) are rather circular, as could be expected, whereas for the chosen $R\theta$ -model they have a flat elliptical shape. This behaviour is plausible when remembering the conditions which have to be met by this model:

- (a) preservation of area;
- (b) preservation of the radial (and azimuthal) midpoint;
- (c) agreement between pin radius and the distance between the radial midpoint and the midpoint of the azimuthal flat.

The noncircular shape is due to the fact that the azimuthal extension is too large as compared with the radial extension. This situation could be improved by requiring instead of condition (c) above, the modified condition

(c') that the distances between the radial midpoint and the closest points on the radial and azimuthal surfaces have to be equal. One could hope that in this way the corresponding contour lines would become more circular.

However, when looking at the consequences of this alternative condition one becomes aware that its realization means that probably too much absorber material is placed close to the surface of the rod (i.e., moved in outward direction). This induced rearrangement of material might lead to an increased effectiveness of the absorber (too much material too close to the fuel region surrounding the absorber rod).

To improve the situation in this respect it seems conceivable that instead of preserving the radial midpoint, it might be more suitable to preserve the centre of gravity, i.e., to require that

(b') the mass centre of the "pseudo-pin" in R Θ -geometry should agree with the position of the real pin centre. Fulfilment of this condition probably improves the chance of being able to keep the local flux minimum within the absorber region approximately at the same position for the R Θ -model as for the real pin configuration of the absorber rod.

One could imagine that an alternative proposal for an even more representative R Θ calculational model could be suggested on the basis of the above conditions (a), (b'), and (c'), i.e.,

- (I) preservation of absorber area;
- (II) preservation of the mass centre;
- (III) equal shortest distances between the midpoint (not centre of gravity) and all external surfaces of the "pseudo-pin".

In summary it is evident that several possibilities of combining plausible requirements are existing. The most appropriate choice among them may presumably depend on the particular problem considered. But - apart possibly from exceptional cases - the specific choice taken for a certain problem will probably not have a really significant influence on the desired results at least for the problem investigated here, namely the homogenized reactivity equivalent cross sections for the SAC to be used eventually for whole core calculation of SPX-1.

3.2 Homogenization of the Control Rods

After having obtained the bare rod worths for the lower and upper SAC, we now have to produce equivalent homogeneous cross sections to be used as input for the final whole core calculations. The general strategy to do this has already been described in section 2; we now present the details, starting with the computation of "first estimate" cross sections, followed by the adjustment procedure using the transport SAC reactivities as a reference.

3.2.1 Calculation of First Estimate Homogeneous Cross Sections.

To obtain a first set of homogenized macroscopic cross sections, we apply the multi-group neutronics code KAPER4 /9/, which solves the one-dimensional integral transport equation with isotropic scattering (using the transport approximation) by a collision probability formalism. With the nuclear data library KFKINR /10/ as basis, neutron fluxes are calculated in 26 energy groups for a cylindrical singularity. Heterogeneity-corrected homogeneous cross sections are then produced in a similar way as in the old supercell model; however, in the new supercell model the control rod regions are represented somewhat differently. In both the lower and the upper SAC cases, the absorbers are described by rings, with areas equalling those of the eight and four pins, respectively, and with material compositions as in the TWODANT calculations. The steel sheath surrounding the control rod is not explicitly taken into account, but via replacing the sodium by a homogeneous mixture of follower and sheath material. Sketches of the rod models are given in Fig. 9. As in the earlier KfK-analysis (see section 2), the absorber cells are surrounded by a fuel annulus of 20 cm thickness, using a white boundary condition on its outer surface.

Cross sections for the sodium follower were produced using the same type of supercell calculation. It is important to note, however, that for sodium-followers - such as for low density regions in general - KAPER4 produces so-called effective diffusion coefficients. Their use in place of the usual values $D = 1/3 \Sigma_{tr}$ leads to a substantial improvement in the treatment of axial neutron leakage in diffusion theory calculations. Thus, the treatment of the follower configuration in diffusion calculations can be considered sufficiently reliable. Errors in calculated rod worths observed later (see next section) can therefore be predominantly attributed to poor cross sections for the absorber parts.

It should be mentioned that in accordance with the earlier method, the neutron fluxes and resulting homogenized cross sections are not calculated through an eigenvalue search, but through a buckling iteration with a target eigenvalue of 1.0.

3.2.2 Adjustment of the Homogeneous Cross Sections

With the set of homogenized cross sections for the follower and both SACs, again control rod worths are computed. Although the calculations are performed for the bare follower and SACs (i.e. embedded in a large cylinder of core material with the same radius as in the reference transport model, cf. Fig. 3), this is done in close resemblance to the final whole core calculations, in the following sense: (a) the diffusion code D3D/D3E is applied; (b) the same energy condensation scheme is used as in the whole core runs; (c) a coarse spatial mesh is chosen, with widths similar to the final ones; (d) the calculations are performed in three dimensions with a height identical to that of the actual reactor core.

The multiplication constants resulting from this "homogeneous diffusion model" are given in Table 4a and the reactivity differences between follower and SAC in Table 4b (last lines for both cases), along with the corresponding values obtained using transport theory (first lines). It is recognized that the reference rod worths are vastly overestimated by the homogeneous diffusion model results. Also displayed are multiplication constants and reactivity differences resulting from various intermediate calculations, passing step by step from the reference to the whole-core like runs, such that the influences of the various changes of the calculation types can be observed separately. That is, entry (1) presents the results of the reference transport model calculations, as already given in Table 2. Entry (2) contains the results of a completely analogous calculation (same geometry, material compositions, cross sections, etc.) performed in diffusion approximation. Entry (3) again refers to a diffusion calculation with the only difference that the geometry has been changed: The absorber sections are replaced by rings similarly as in the new supercell model of Fig. 9. At this point, it is interesting to note that the considerable rod worth discrepancies appearing in diffusion calculations when passing over to the ring model are not observed in transport theory; there, the differences are approximately half as large. In entry (4), the follower and rod regions are replaced by a homogeneous area, with cross sections calculated with the KAPER4 code as described in the previous subsection. In entries (5) and (6), transitions are performed from 26 to 4 energy groups, and from a fine to a coarse grid, respectively. All these entries refer to two-dimensional $R\theta$ calculations with a constant buckling of $8.62 \times 10^{-4} \text{ cm}^{-2}$ to account for the axial leakage. The finite height (100 cm)

is finally taken into account in entry (7), which displays the results of a three-dimensional R θ Z diffusion calculation.

The differences of the rod worths resulting from the diffusion approximation, homogenization, energy group condensation, spatial grid coarsening, and transition to three dimensions, as well as the sums of these effects altogether, are compiled in Table 4c. It is seen that the main contributions to the discrepancies between the reference and the whole-core like results arise from the diffusion approximation, and, to a smaller degree, from the homogenization of the cross sections. The remaining differences are almost negligible, and so is the S_n-order effect in the reference calculations which had been addressed in subsection 3.1.3.

From the preceding discussion it is evident that a diffusion calculation of the form described above is not adequate for the whole core situation without further modification, due to the inability to produce reliable results for a much simpler arrangement. Since it is not possible, at the present level of computational methods available, to perform the whole core calculations at a similarly high numerical level as the reference calculations, appropriate changes have to be made such that the low level of the homogeneous diffusion calculations is retained, but its accuracy and reliability are improved.

An obvious method to improve the results of the diffusion calculations is to adequately modify the input homogeneous cross sections. This is done in such a way that the reference rod worths are reproduced by the homogeneous diffusion model calculations. That means that all the influences leading to the discrepancies between the heterogeneous transport and the homogeneous diffusion results are compensated by using equivalent homogeneous macroscopic cross sections. Because these diffusion calculations are performed on the same numerical level as the final whole core calculations, it is supposed that these cross sections are also appropriate to be used as input for the SAC cells in the final runs.

Since the rod worths in the homogeneous approximation are too large in comparison with the reference transport model values, the absorption components in the cross sections have to be diminished. This should be done in a physically reasonable way, i.e. the set of cross sections should be consistent. To ensure this, we generate new cross sections through homogenization of a physically possible heterogeneous arrangement, by again employing the collision probability code KAPER4 as was de-

scribed for the new supercell model in subsection 3.2.1, with modified input data. In order to introduce as little arbitrariness as possible, we leave the once chosen geometries unchanged and alter the material compositions only. Thus, a decrease of the reactivities of the control rods can be achieved by reducing the boron carbide concentrations in the absorber regions below their actual values. This is done independently for the lower and upper SACs. The homogenized cross sections generated in this way are used again as input for the homogeneous diffusion model calculations described above. The absorber concentrations finally chosen are fixed by requiring that the rod worths obtained within the homogeneous diffusion calculations agree with the reference transport model values.

In Fig. 10, it is shown how a reduction of the boron carbide concentration influences the reactivity differences between sodium follower and control rods in the homogeneous diffusion model. The concentrations are normalized to the actual ones. Also plotted are the reference rod worths from the detailed transport calculations. The intersections of the curves with these horizontal lines indicate the absorber concentrations required for generating the desired homogeneous cross sections. It can be seen that the boron carbide has to be diluted to 62 % of its original amount for the lower SAC and to 48 % for the upper SAC. To get an impression of the influence of the reduction of the boron carbide concentration on the homogenized macroscopic cross sections, we display in Table 5 the corresponding numbers, calculated within four energy groups, for the lower SAC before and after the modification (100 % / 62 % B_4C). Especially in group 4, it is obvious that the homogenized effective capture cross section is not reduced by the same amount as the absorber concentration. This is due to the fact that with reduced absorber concentration, the spatial flux depression becomes less pronounced so that the effectiveness of the inner parts of the absorbers increases, and correspondingly the effective specific macroscopic capture cross section (per absorber atom) increases, too, so that the reduction of the effective capture cross section is not as pronounced as the associated reduction of the absorber concentration.

Obviously, by reducing the boron carbide concentration, the total density inside the absorber pins is reduced also, which decreases the macroscopic cross sections. This decrease of the transport cross section reduces the optical thickness and the transparency of the absorber region. One cannot exclude a priori that such a change of the neutron mean free path in certain ranges of the control rod could have some influence

on its overall characteristic nuclear parameters, like e.g. the reactivity worth. Therefore, we have performed supplementary calculations by reducing the boron-10 enrichment instead of the boron carbide concentration, such that the total amount of boron as well as carbon remains constant. It was found that this procedure does not produce any significant changes of the results. Hence, we conclude that the reduction of the boron carbide concentration is appropriate for our present purpose.

4 RESULTS OF THE WHOLE CORE DIFFUSION CALCULATIONS FOR SPX-1

The homogeneous macroscopic SAC cross sections thus generated are employed now to perform calculations for the fully loaded power production SPX-1 core in diffusion approximation. As already mentioned, a rather coarse discretization of the energy and space variables is used, namely four energy groups and seven mesh points per unit hexagon. The remaining cross sections needed for establishing the input data set (core elements, blanket elements, etc.) were taken from earlier homogenization calculations /2/. The cross sections for the main control system SCP have been generated recently in a similar way as for the secondary shut-down system /19, 20/.

According to the homogenization procedure described above, the SAC cross sections already contain a large part of the corrections usually required as a consequence of the coarse energy and space discretization; therefore, any additional corrections to account for these effects are not necessary in our present approach.

We have computed reactivities in two and three spatial dimensions. The two-dimensional calculations merely serve to demonstrate how the rod worths in the whole core arrangement change with decreasing boron concentration. In this case, the D3D/D3E code is run separately for the lower and the upper SAC, since in two-dimensional hexagonal geometry the axial structure cannot be taken into account. In Fig. 11, the ratios of the reactivity differences between the arrangements with inserted and withdrawn SAC rods at 100 % and those at varying B₄C concentration are displayed at critical SCP insertion depth. (For the two-dimensional runs, "critical SCP insertion depth" actually means that the absorber content of the homogeneous SCP mixture has been reduced from its actual value by such an amount that the multiplication constant equals unity when no SAC rod is present.) These curves can be compared with the C/E value (ratio of calculated to measured reactivity worth) resulting from the old calculations, which is also shown in Fig. 11. It is recognized that with the "best" concentrations of 62 % for the lower and 48 % for the upper SAC, the calculated ratios come close to the old C/E ratio, which means that with our new cross sections the original discrepancies between the computed and the measured SAC rod worths can be approximately compensated.

In Table 6, we finally present the results of the fully three-dimensional whole core diffusion calculations. The computed reactivities of the secondary shut-down system are again compared with the measured values for the same SCP insertion depths as in Table 1. We observe an essential improvement in reproducing the experimental reactivities as compared with the earlier calculations. With the new homogenized SAC cross sections, the original discrepancies between the computed and the measured reactivities of approximately 20 % are reduced to 1 % for critical and 2 % for full SCP insertion depth. We again note that these results have been obtained by using a rather coarse space and energy discretization and without explicitly applying any corresponding corrections, according to the philosophy that the corrections necessary for compensating the mesh and condensation effects are already performed implicitly by our choice of the procedure to derive homogeneous macroscopic cross sections.

5 CRITICAL REMARKS ON THE USED BUCKLING

In the reference transport model calculations, only horizontal cuts through the control rod parts were modelled in detail, whereas their finite heights could not be properly taken into account since the TWODANT code does not provide the capability of a full treatment of three-dimensional problems. Rather, the macroscopic cross sections were modified with buckling corrections. This buckling was determined from diffusion calculations, in such a way that the axial leakage is approximately taken into account within the framework of the diffusion approximation. It is not a priori evident, however, that the resulting buckling value is equally well suited for transport calculations. Furthermore, a global, i.e. material- and energy-independent buckling was used for the complete arrangement under consideration (singularity and surrounding core zone), assuming the same value for the follower and absorber singularities. The buckling values may have some influence on the magnitude of the reactivity effect caused by replacing the follower by an absorber. This influence results from the fact that for an accurate determination of such type of reactivity worths it is of crucial importance to approximate the neutronic weight of the singularity acceptably for both cases, i.e. the follower and the absorber configuration. Due to the low absorption cross section of the follower material, the axial leakage - represented by corresponding buckling values - has a dominant influence on the neutronic weight of the singularity for the follower configuration.

To obtain buckling values which are more suited for our purposes, one could imagine the following refined method, which was investigated in a second step of our studies.

As a first step, transport calculations are performed for a cylindrical arrangement consisting of fuel material only (with the same radius as in the reference transport model calculations for follower and SACs, and vacuum outer boundary conditions, see Fig. 3). These calculations are performed (a) in RZ geometry with a core height of 100 cm and vacuum boundary conditions on the horizontal surfaces, and (b) in R θ geometry using buckling modified macroscopic cross sections. The buckling is adjusted by requiring that both calculations yield identical multiplication constants, leading to a numerical value of $B^2 = 8.36 \times 10^{-4} \text{ cm}^{-2}$, not much deviating from the one originally used ($8.62 \times 10^{-4} \text{ cm}^{-2}$), which was derived from diffusion calculations.

Then, TWODANT calculations are performed for the sodium follower and the control rod singularities, again in RZ and R Θ geometries. For this purpose, simplified cylinder symmetrical rod models (similar as in the new supercell model, cf. Fig. 9, but with an outer radius of the fuel zone of about 120 cm) are established, which is necessary for using RZ geometry. In the R Θ cases, material dependent bucklings B_F^2 and B_S^2 are used, being different for the fuel zone and the singularity. The numerical values are determined by the following two requirements:

- a) the multiplication constants agree for the RZ and R Θ calculations;
- b) the ratios between ϕ_S , the flux summed over energy groups and averaged over the singularity region, and ϕ_F , the flux summed over energy groups and averaged over the fuel region, agree for the RZ and R Θ calculations.

Fortunately, it turns out that the value obtained for the cylinder consisting of fuel only can be kept as buckling for the fuel region in each case; by adjusting the bucklings for the singularity regions both requirements a) and b) can be satisfied simultaneously with sufficient accuracy.

The bucklings resulting for the singularities are given in Table 7; it can be seen that for all cases the values for the singularities differ appreciably from the value for the fuel material. Also shown are the multiplication constants, the reactivity worths against the sodium follower, and the fluxes ϕ_S and ϕ_F , averaged over the singularity and the fuel regions, respectively, as well as their ratio.

The results given in Table 7 were determined with S_4 calculations. It should be mentioned that by increasing the S_n order to 16, the results for the rod worth do not change substantially. (Furthermore, one could imagine to derive group- or even group- and space-dependent buckling values by analogous procedures which are somewhat more complicated. We have disregarded such possibilities since the described simple treatment turned out to be sufficient for our purpose).

Finally, it is assumed that the bucklings obtained for the ring-shaped singularities can be taken over for the reference transport model displayed in Fig. 3. This seems reasonable since the amounts of coolant (as well as absorber) are equal for both the simplified and the detailed models. This argument is supported by the fact that the

buckling value is of particular importance for the coolant regions (and of smaller importance for the absorber parts) so that it is reasonable to attribute the same buckling values to the coolant sections of all models.

The results of the reference transport model calculations with macroscopic cross sections modified according to these material dependent bucklings are also given in Table 7. A rise of the reactivity differences between follower and SAC as compared with our original "reference" rod worth is observed. This rise in turn causes an increase of the adjusted boron carbide concentrations to be used for generating equivalent homogenized cross sections (75% of the actual value for the lower and 62% for the upper SAC, as can be seen from Fig. 10 by replacing the reference values, which resulted in "best" concentrations of 62 % for the lower and 48 % for the upper SAC, by those displayed in Table 7).

From these findings we conclude that the concept of a material-independent buckling is not completely adequate in the form as it was used in our reference transport model (see subsection 3.1.2). At this point, one has to note that for deriving DB^2 the unmodified transport cross section or the correlated diffusion constant as calculated with GRUCAL was used. It is known, however, that the use of modified transport cross sections generated with KAPER4 in the supercell option for neutronically thin media substantially improves the description of the leakage conditions in diffusion calculations. Therefore, we have produced macroscopic cross sections for the sodium follower according to a material-independent buckling of $8.36 \times 10^{-4} \text{ cm}^{-2}$, using the KAPER4 instead of the GRUCAL transport cross sections. This yields a reactivity difference of 711.8 pcm between the fuel cylinder and the follower in a two-dimensional S_4 transport calculation. To obtain this value, direction-dependent macroscopic transport cross sections had been generated with KAPER4 (cf. Ref. /9/, p. 51), and the axial transport cross section $\Sigma_{lr,ax}$ from this KAPER4 run was then used to establish the axial leakage term in the two-dimensional transport calculation. It turned out, however, that in this case the distinction of the axial and radial directions has only a minor influence on the result for the reactivities: using the direction-independent transport cross section, the reactivity difference between fuel and follower is 704.5 pcm.

It should be mentioned that the KAPER4 cross sections were homogenized over the regions of the follower and the surrounding steel sheath, and accordingly, in the corresponding transport calculation a mixture of sodium and steel was used for both the fol-

lower and the sheath regions. When the individual regions are described separately, however, the multiplication constant is hardly influenced, yielding a reactivity difference of 705.4 pcm with the axial KAPER4 transport cross section used for deriving DB^2 . The results obtained with the different treatments of the follower and sheath regions, and with different types of buckling corrections are compiled in Table 8.

When using the GRUCAL transport cross sections for performing the buckling correction, the reactivity worth is 909.1 pcm. Comparing with the reactivity difference of 718.3 pcm resulting from the RZ model, which can be determined from Table 7, shows sufficient agreement between the reactivity differences in the RZ and the R θ model with a material-independent buckling on the basis of the KAPER4 transport cross sections, confirming the adequacy of the refined method described above. In a preliminary step, we had verified the suitability of such a treatment for one-dimensional models, i.e. for $B_{ax}^2 = 0$, assuming an infinite extension of the configuration in the axial direction.

However, it should be noted that the modelling of the SAC control rod is not yet completely satisfying with both of the methods described, since the presence of other absorbers or structure materials above or below the SAC part under consideration is not accounted for. At present, we cannot satisfactorily treat this problem, since this would require the use of an appropriate fully three-dimensional transport code, with the capability to model the internal structure of the SAC in sufficient detail, cf. Fig. 1.

We have finally calculated homogenized macroscopic cross sections with effective boron concentrations of 75 % and 62 % of the actual value for the lower and the upper SAC, respectively. Using these cross sections as input for the SAC control rods, three-dimensional whole-core diffusion calculations were performed as described in section 4. The results of these calculations are shown in Table 9. One observes that with respect to Table 6, calculated rod worths now increased by approx. 9 %, and that therefore the previously very favourable agreement between theory and experiment is somewhat deteriorated. Although C/E ratios now range from 1.06 to 1.10, it is important to note that even with the use of these cross sections, a substantial improvement is still obtained with respect to the earlier SPX-1 calculations on the basis of actual absorber concentrations, where C/E ratios ranged from 1.17 to 1.23 /20/.

6 SUMMARY AND OUTLOOK

We have presented an improved approach for the numerical evaluation of control rod reactivity worths in fast sodium cooled nuclear reactors. While BELGONUCLEAIRE (BN) had already successfully used this method for the prediction of the worth of the main control system SCP (système de commande principale) in SUPERPHENIX-1 (SPX-1), it was now applied to the control rods of the secondary shut-down system SAC (système d'arrêt complémentaire) of the same reactor. The important aspect of the present GRS/KfK evaluation is in that the geometry of the SAC absorbers is much more heterogeneous than that of the formerly treated SCP absorbers and that the present work therefore represents a much more rigorous test of the new method.

The motivation for the development of this new method was the following: Whole core reactor analysis calculations for the prediction of control rod worths are usually run in diffusion theory, using a relatively coarse mesh grid and nuclear cross sections condensed to few energy groups. Rod worths obtained from such calculations are consequently affected by a number of so-called 'approximation'-errors and a-posteriori corrections for transport, condensation, and mesh-size effects are applied to render the results more trustworthy. Unlike transport corrections on rod worths, which were always found to be rather insensitive to rod positions and individual rod configurations, condensation and mesh-size corrections are strongly configuration dependent and have to be re-assessed for each rod pattern. After running through this elaborate standard calculation procedure, the SPX-1 analysis showed that control rod worths were substantially overestimated with C/E ratios ranging from 1.17 to 1.23, while representative earlier experiments had given values between 1.00 and 1.10 /2,3/. For cores of larger fissile diameter a trend had been found towards the upper end of this spectrum of values, whereas for smaller cores C/E ratios were close to unity or even somewhat below. The principal reason for the particularly substantial overprediction of control rod worths in SPX-1 was found to lie in the standard method of producing homogeneous cross sections for the control rod absorbers, in which subregion cross sections of a simplified cylindrical model of the absorber are averaged via flux-volume weighting. Weighting fluxes are taken from a 'supercell' calculation in 1D radial geometry (absorber in the centre of a fuel cylinder) using the collision probability code KAPER4. The inadequacy of this procedure in the case of SPX-1 is a consequence of the extremely heterogeneous structure of its control rods, the complex absorption be-

haviour of which is unlikely to be properly accounted for by a cylindrical model, where the choice of the material distribution was solely ruled by geometrical considerations.

Although over the years, mainly in the UK /4/ and in Japan /7/ more sophisticated schemes have been developed for the preparation of more reliable homogenized absorber cross sections, most of these still rely on cylindricalised absorber models and thus to a certain extent on the arbitrary choice of the evaluator. Apart from the fact that the special codes used in this context were unavailable to BN and GRS/KfK, it was not considered useful to still adhere to cylindrical models. A new simple approach was therefore developed which could rely on existing computer codes, especially on a transport code in R θ -geometry, which allowed a realistic modelling of the absorber layout.

The basic idea behind this new approach was to produce and adjust a set of homogeneous absorber cross sections in such a way that a calculation using these cross sections would give the same reactivity effect relative to a sodium follower as a so-called 'reference' calculation in which the internal structures of this absorber are modelled as precisely as possible. Particularly attractive seemed the idea of running the calculation using the homogeneous cross sections on a level corresponding to that of the standard whole core analysis calculations (few-group diffusion with coarse meshes); the 'reference' calculation, however, in transport theory and with a fine energetic and spatial resolution. Imposing equality of the reactivity effects would then result in adjusted homogeneous cross sections that do not only account for absorber heterogeneity (obviously only in a global reactivity-oriented way and not in a microscopic picture), but also for the effects of energy group condensation and coarse mesh spacing. A use of such cross sections in the standard analysis calculations would therefore substantially facilitate rod worth predictions since a-posteriori corrections would become largely obsolete.

Since the 'reference' calculations form the basis of the present cross section adjustment, they should resemble experimental reality as closely as possible. In particular the control rod in its detailed representation should be exposed to a realistic flux spectrum and profile. In practice, however, only part of these different requirements can actually be satisfied: In the case of the SPX-1 control rods it was found that the internal absorber structures could best be modelled in R θ -geometry, while the global reactor grid has triangular (hexagonal) geometry. Since the deterministic codes used by

GRS/KfK do not allow a mixing of different types of geometry (as do Monte Carlo codes) one was forced to simplify the core surrounding the control rod of interest. As a compromise, the control rod absorber or sodium follower, respectively, were therefore simply inserted into a bare fuel cylinder.

It is worth noting that even if the interior of the control rod had been amenable to a description in hexagonal or triangular geometry, the deterministic codes in use would have required an extension of the fine mesh grid, basically necessary only for a sufficient spatial resolution of the absorber, to the whole reactor, leading to intolerable computer space and time requirements. This undesired high spatial resolution in regions where it is largely irrelevant could only be avoided by application of specially tailored codes, which have particular options for taking into account the internal structure of a control rod subassembly, either directly or by simulating it, e.g. by suitably chosen internal boundary conditions or by equivalent special response matrices.

A more severe limitation arose from the unavailability of a suitable 3D transport code. This had the consequence that in the 'reference' calculations radial and azimuthal details of the internal absorber structures could be well represented, axial composition variations, however, could not be accounted for (see Fig.1). While in the case of the SCP-absorber and of the sodium follower, axial neutron propagation could be sufficiently well described by a suitable axial buckling as both have uniform axial material distributions, this method becomes extremely questionable in the case of the presently investigated SAC-absorbers. These consist of a 'train' of axially articulated absorber units with two different types of absorber arrangements. As such axial material variations could not be directly modelled, it was decided to run two individual 'reference' calculations, one for each type of SAC absorber unit, thus representing horizontal cuts through the SAC absorber at different heights. In these calculations the existence of axial heterogeneities was thus neglected and axial neutron leakage again described by a global axial buckling.

The next step was to produce homogeneous absorber cross sections following the standard procedure. Using cylindricalized models of the two types of SAC absorber units, homogeneous, direction-independent cross sections were produced for each of the models annular subzones. For each of the two absorber units, these subregion cross sections were combined by flux-volume weighting to give one set of homogenized cross sections for this particular absorber unit. The weighting fluxes were taken

from one-dimensional supercell calculations performed with a collision probability code in which the cylindricalized models of the two absorber types were implanted into a fuel cylinder with reflective outer boundary. A third supercell calculation was run to produce cross sections for the sodium-follower. It is important to note that although, here again, homogeneous cross sections were produced on the basis of cylindrical models, these cross sections only represent a first guess and will later be modified.

Using the so obtained homogeneous cross sections, the reactivity worth of the two SAC absorber units relative to a sodium-follower was determined in the same simple cylindrical arrangement as in the reference calculations (central absorber or follower in a fuel cylinder). To include transport, condensation and mesh corrections in the intended cross section adjustment, these homogeneous calculations were run on the level of the whole core analysis calculations, i.e in diffusion theory using few energy groups and a coarse mesh grid. It was found that these homogeneous rod worths were significantly greater than the worths found in the 'reference' calculations.

To obtain absorber cross sections with the proper absorbing strength or the correct neutronic weight of the central region of the arrangement, the production of the homogeneous cross sections was re-run and iteratively repeated with artificially reduced boron carbide concentrations until the homogeneous calculations reproduced the 'reference' rod worths. It was found that the necessary absorber concentration reductions were similarly substantial as that found by BN /20/ for the SCP-rods (56.5% of the original density): SAC upper link absorber: 48%, SAC lower link absorber: 62%.

A new campaign of SPX-1 whole core analysis calculations was then launched, in which these new adjusted homogeneous cross sections were used for the SAC control rods. It should be noted that in contrast to the SCP-rods, where the adjusted homogeneous cross sections were used over the full radial and axial extension of the absorbers, the different axial absorber units of the SAC-rods were 'filled' with their individually associated homogeneous cross sections. Structural parts between the different absorber units used simple unadjusted homogeneous cross sections.

The new calculations produced C/E ratios for the SAC rods close to unity, and thus similar to the SCP rod worth predictions found with the adjusted cross sections of BN and in good global agreement with earlier experiment analyses.

In the previously described evaluation, the axial leakage in the R θ 'reference' calculations was treated by a representative axial buckling B_{ax}^2 . For both, the follower and absorber cases, the usual homogeneous diffusion constant D was used to determine the leakage contribution DB_{ax}^2 .

As an alternative method to derive 'reference' reactivity worths from 2D transport calculations, the sodium follower or one of the absorbers were placed into the centre of an RZ model. Reactivity worths obtained in this way were found to differ from those originally calculated. Supplementary studies then showed that a use of direction dependent diffusion constants, in particular D_{ax} from KAPER4 for the axial direction of the R θ models leads to an improved agreement of the 'reference' reactivity worths deduced from R θ and RZ transport calculations, but resulted in higher 'reference' worths than the previous evaluation. This is due to the fact that the neutronic weight of the follower region changes when using $D_{ax} B_{ax}^2$ instead of the usual DB_{ax}^2 . As a consequence of the now obtained higher 'reference' worths, the absorbers in the homogeneous cross section production had to be less diluted to match the 'reference' worths (upper SAC absorber: 62%, lower SAC absorber: 75%) and consequently C/E ratios for the SAC absorbers increased to values between 1.06 and 1.10, depending on the insertion state of the SCP-rods. Although this result somewhat deteriorated the consistency with the C/E ratios found for the SCP-rods, one has to see that the layout of the SAC rods is much more complicated. In the case of the SAC-rods, the different approximations introduced in the present approach might therefore well have a more severe impact on the reliability of the results.

In a more global view, one finds that even the increased SAC C/E ratios still fit very well into the range of earlier observed C/E ratios between 1.0 and 1.1; in particular as large cores always showed a trend towards the upper end of this range /2,3/.

Putting finally the new approach presented here into a more general perspective, one should not forget that despite the very favourable results obtained with respect to the first SPX-1 analysis using standard methods, the present cross sections are the result of a relatively crude adjustment procedure involving substantial simplifications of the realistic experimental situation: In the reference transport calculations, e.g. the absorbers in question were embedded into the centre of a clean fuel region without any spectral perturbations from other control rods or zone boundaries and without a radial

flux gradient to which off-centre rods in a real reactor are exposed. Obviously, even the existing advanced methods mentioned before suffer from this shortcoming. The question therefore arises, how well parameters like neutronic 'albedo' and 'transparency' in differently distorted flux spectra and profiles can really be tuned into the homogenized cross sections of a simple supercell model and what the role of compensating errors might be.

Furthermore, the present method assumes the correctness of the sodium follower cross sections and subjects therefore only the absorber cross sections to an adjustment procedure. Although the use of adequately modified diffusion coefficients /21/ for the sodium followers does indeed justify this assumption to a large extent, residual errors in the treatment of follower neutron leakage will persist in whole core calculations. These residual errors, however, are expected to be small and the fact that they are 'tuned' into the absorber cross sections is unlikely to have a severe impact on the present results.

In conclusion we might state that although the present new approach to produce homogeneous cross sections for strongly heterogeneous control rod absorbers is based on a substantial number of simplifying assumptions, its successful use in the SPX-1 analysis suggests further validation in other experiments and a tentative application for design level calculations of future reactors.

ACKNOWLEDGEMENTS

S. Langenbuch and W. Zwermann gratefully appreciate the kind hospitality experienced during their stays at KfK. The authors would like to thank Drs. G. Buckel and B. Stehle for their help in applying the specific codes.

REFERENCES

- /1/ "La centrale à neutrons rapides de Creys-Malville (Super-phénix)"
CEA Bulletin d'Informations Scientifiques et Techniques, Vol. 227, pp. 69-72, 1978
- /2/ U.K. Wehmann, H. Giese
"Methods for Shut-down Worth Calculations in Fast Reactors and their Validation with Help of SPX-1 Absorber Experiment Evaluations"
Proc. IAEA/IWGFR Specialists' Meeting on Methods for Reactor Physics Calculations for Control Rods in Fast Reactors, Winfrith, UK, Dec. 6 - 8, 1988, pp. 341-353
- /3/ H. Giese, S. Pilate, J.M. Stevenson
"Worths and Interactions of Simulated Fast Breeder Reactor Control Rods in ZEBRA and SNEAK Assemblies"
Nucl. Sci. Eng., Vol. 87, pp. 262-282, 1984
- /4/ J.L. Rowlands, C.R. Eaton
"The Spatial Averaging of Cross Sections for Use in Transport Theory Reactor Calculations, with an Application to Control Rod Fine Structure Homogenization"
Proc. Specialists' Meeting on Homogenisation Methods in Reactor Physics; Lugano, Switzerland, Nov. 13 - 15, 1978, pp. 261-268
- /5/ J.C. Cabrillat, M. Carta, H. Giese, G. Palmiotti, V. Peluso, M. Salvatores
"Application of Transport Equivalent Cross Sections Obtained by the MONSTRE Method to SPX-1 Case"
Proc. IAEA/IWGFR Specialists' Meeting on Methods for Reactor Physics Calculations for Control Rods in Fast Reactors, Winfrith, UK, Dec. 6 - 8, 1988, pp. 263-285

- /6/ G. Palmiotti
"A Method to Obtain New Cross-Sections Transport Equivalent"
Proc. IAEA/IWGFR Specialists Meeting on Methods for Reactor Physics Calculations for Control Rods in Fast Reactors, Winfrith, UK, Dec. 6 - 8, 1988, pp. 33-56
- /7/ T. Takeda, N. Uto
"Comparison of Cell Homogenization Methods Considering Interaction Effects between Fuel Cells and Control Rod Cells"
Proc. IAEA/IWGFR Specialists' Meeting on Methods for Reactor Physics Calculations for Control Rods in Fast Reactors, Winfrith, UK, Dec. 6 - 8, 1988, pp. 57-83
- /8/ P. Benoist, M. Carta, G. Palmiotti, M. Salvatores, J. Tullet
"A Simple Calculation of Control Assembly Effectiveness in a Liquid-Metal Fast Breeder Reactor by a Transport-Diffusion Equivalence Method"
Nucl. Sci. Eng., Vol. 103, pp. 254-264, 1989
- /9/ R. Böhme, E.A. Fischer
"The Fast Reactor Cell Code KAPER4"
KfK-4435, Kernforschungszentrum Karlsruhe, 1988
- /10/ E. Kiefhaber
"The KFKINR-Set of Group Constants, Nuclear Data Basis, and First Results of its Application to the Recalculation of Fast Zero-Power Reactors"
KfK-1572, Kernforschungszentrum Karlsruhe, 1972
- /11/ B. Stehle
"D3D und D3E. Zweige eines FORTRAN-Programms zur Lösung der stationären dreidimensionalen Multigruppenneutronendiffusionsgleichungen in Rechteck-, Zylinder- und Dreieckgeometrie"
KfK-4764, Kernforschungszentrum Karlsruhe, 1991

- /12/ R.E. Alcouffe, F. W. Brinkley, D.R. Marr, R.D. O'Dell
 "User's Guide for TWODANT: A Code Package for Two-dimensional, Diffusion-Accelerated, Neutral-Particle, Transport" (Revision 1.3)
 LA-10049-M, Los Alamos National Laboratory, 1986
- /13/ D. Woll
 "GRUCAL. Ein Programmsystem zur Berechnung makroskopischer Gruppenkonstanten"
 KfK-2108, Kernforschungszentrum Karlsruhe, 1975
- /14/ G. Buckel, W. Höbel
 "Das Karlsruher Programmsystem KAPROS - Teil 1: Übersicht und Vereinbarungen. Einführung für Benutzer und Programmierer."
 KfK-2253, Kernforschungszentrum Karlsruhe, 1976
- /15/ H. Bachmann, S. Kleinheins
 "Das Karlsruher Programmsystem KAPROS Teil 2: Dokumentation des Systemkerns."
 KfK-2254, Kernforschungszentrum Karlsruhe, 1976
- /16/ "Kurzbeschreibung des KAPROS-Moduls SIGMUT"
 Private Communication
- /17/ "Kurzbeschreibung und Benutzeranleitung der KAPROS-Prozedur DIXY2"
 Private Communication
- /18/ "Kurzbeschreibung des KAPROS-Moduls SIGMNC"
 Private Communication
- /19/ J.C. Cabrillat, M. Carta, A. d'Angelo, H. Giese, R. de Wouters, T. Newton, P. Harrison, M. Salvatores, H. Sztark, U. Wehmann
 "Common Lessons Drawn from Different Laboratories Analyses of Super-Phenix Start-up Experiments"
 Proc. International Conference on the Physics of Reactors: Operation, Design and Computation, Marseille, France, April 23 - 27, 1990, Vol. 1, pp. VII-10 - VII-20

/20/ H. Giese, E. Kiefhaber, R. de Wouters, M.P. Fontaine
"A Novel Approach for the Production of Homogenized Control Rod Absorber Cross Sections and its Application to the Analysis of the Super-Phenix-1 Start-up Experiments"
Proc. International Conference on the Physics of Reactors: Operation, Design and Computation, Marseille, France, April 23 - 27, 1990, Vol. 2, pp. X-35 - X-47

/21/ E.A. Fischer
"Neutron Streaming in Fast Reactor Slab Lattices and in Cylindrical Channels"
Nucl. Sci. Eng., Vol. 78, pp. 227-238, 1981

APPENDIX: LIST OF USED NUMERICAL PROGRAMMES

In this Appendix, we give a brief survey of the mainly used computer codes with respect to their application in the present investigation.

A. TWODANT

Features: Two-dimensional transport code in XY-, RZ-, and R Θ -geometry

Utilization: R Θ -version for detailed control rod models.

Input: Geometry and macroscopic cross sections.

Output: Multiplication constants and neutron fluxes.

B. KAPER4

Features: One-dimensional collision probability code in cylindrical and slab geometry. Isotropic scattering is assumed using the transport approximation.

Utilization: Cylindrical supercell option, i.e. for a cylindrical singularity in core material.

Input: Geometry, particle number densities, and microscopic cross sections (KFKINR-library).

Output: Macroscopic cross sections, homogenized over the singularity, to be used as input for diffusion calculations.

C. D3D/D3E

Features: Three-dimensional diffusion code in XYZ-, R Θ Z-, and hexagonal-Z-geometry.

Utilization: R θ Z-version for detailed and homogeneous control rod models and hexagonal-Z-version for whole core calculations.

Input: Geometry and macroscopic cross sections.

Output: Multiplication constants and neutron fluxes.

D. Others

GRUCAL: Generation of effective (resonance self-shielded) microscopic and macroscopic cross sections from particle number densities and group cross sections.

SIGMUT: Cross section library management and generation of buckling modified macroscopic cross sections.

SIGMNC: Condensation of macroscopic cross sections.

DIXY2: Two-dimensional diffusion code with mesh-edged discretization XY-, RZ-, or R θ -geometry and associated evaluation routines, used for supplementary diffusion calculations to determine bucklings.

Table 1

SAC reactivity worths measured and calculated using cross sections determined with the old supercell model, at (a) critical, (b) full SCP insertion depth.

	$\Delta\rho_{\text{meas}}$ (pcm)	$\Delta\rho_{\text{calc}}$ (pcm)	$\Delta\rho_{\text{calc}}/\Delta\rho_{\text{meas}}$
(a)	1039	1249	1.20
(b)	1191	1392	1.17

Table 2

Multiplication constants for sodium follower and SACs resulting from the reference transport model (26 energy groups, GRUCAL cross sections, $B^2 = 8.62 \times 10^{-4} \text{ cm}^{-2}$) and corresponding reactivity differences between follower and SAC.

	k-eff	$\Delta\rho$ (pcm)
Na-Follower	0.959853	
Lower SAC	0.948121	1289
Upper SAC	0.944801	1660

Table 3

Multiplication constants and reactivity differences from the reference transport model (4 energy groups, GRUCAL cross sections, $B^2 = 8.62 \times 10^{-4} \text{ cm}^{-2}$) and corresponding diffusion calculations.

	k-eff		$\Delta\rho$ (pcm)	
	transport	diffusion	transport	diffusion
Na-Follower	0.962797	0.958867		
Lower SAC	0.950914	0.944752	1298	1558
Upper SAC	0.947527	0.940657	1674	2019

Table 4

Results of various calculations going from the reference transport calculation to the whole-core oriented diffusion calculation: (a) multiplication constants k-eff; (b) reactivity differences between follower and SAC; (c) differences of rod worths between different types of calculations.

- (1) Transport, broken ring, GRUCAL X-sect., 26 grp, fine mesh, 2-D (RΘ)
- (2) Diffusion, broken ring, GRUCAL X-sect., 26 grp, fine mesh, 2-D (RΘ)
- (3) Diffusion, closed ring, GRUCAL X-sect., 26 grp, fine mesh, 2-D (RΘ)
- (4) Diffusion, homogeneous, KAPER4 X-sect., 26 grp, fine mesh, 2-D (RΘ)
- (5) Diffusion, homogeneous, KAPER4 X-sect., 4 grp, fine mesh, 2-D (RΘ)
- (6) Diffusion, homogeneous, KAPER4 X-sect., 4 grp, coarse mesh, 2-D (RΘ)
- (7) Diffusion, homogeneous, KAPER4 X-sect., 4 grp, coarse mesh, 3-D (RΘZ)

	Na-Follower	Lower SAC	Upper SAC
(a) Multiplication constants			
(1)	0.959853	0.948121	0.944801
(2)	0.956907	0.943271	0.939334
(3)	0.956907	0.943592	0.939970
(4)	0.955372	0.941214	0.937161
(5)	0.957347	0.943180	0.938947
(6)	0.957378	0.943076	0.938759
(7)	0.957327	0.942900	0.938556
(b) Rod worths (pcm)			
(1)		1289.2	1659.8
(2)		1510.7	1955.0
(3)		1474.6	1882.9
(4)		1574.5	2034.0
(5)		1569.0	2047.0
(6)		1584.0	2071.7
(7)		1598.3	2089.1
(c) Rod worth differences (pcm)			
(2)-(1)		221.5	295.3
(3)-(2)		-36.1	-72.1
(4)-(3)		99.9	151.1
(5)-(4)		-5.5	13.0
(6)-(5)		15.0	24.7
(7)-(6)		14.3	17.5
(7)-(1)		309.1	429.3

Table 5

Four-group macroscopic cross sections for the homogenized lower SAC with original and reduced boron carbide concentrations. Units for the cross sections are cm^{-1} . Reduction factors for the capture cross section (i.e. the ratios between cross sections for original and reduced boron carbide concentrations) are also given.

TYPE	GROUP			100% B4C	62% B4C	REDUCTION FACTOR
CHI	1	.	.	5.70000E-01	5.70000E-01	
NUSF	1	.	.	0.0	0.0	
SCAPT	1	.	.	3.12764E-03	2.08385E-03	0.66627
SFISS	1	.	.	0.0	0.0	
SREM	1	.	.	2.28533E-02	2.01176E-02	
STR	1	.	.	8.00317E-02	7.45917E-02	
SMTOT	1	IN	1	8.62762E-02	7.88344E-02	
SMTOT	1	IN	2	1.84968E-02	1.68089E-02	
SMTOT	1	IN	3	1.22436E-03	1.22051E-03	
SMTOT	1	IN	4	4.35182E-06	4.35242E-06	
CHI	2	.	.	3.35000E-01	3.35000E-01	
NUSF	2	.	.	0.0	0.0	
SCAPT	2	.	.	4.05147E-03	2.64456E-03	0.65274
SFISS	2	.	.	0.0	0.0	
SREM	2	.	.	1.95905E-02	1.53157E-02	
STR	2	.	.	1.30177E-01	1.20084E-01	
SMTOT	2	IN	2	1.33010E-01	1.20185E-01	
SMTOT	2	IN	3	1.55350E-02	1.26672E-02	
SMTOT	2	IN	4	4.02158E-06	4.02334E-06	
CHI	3	.	.	9.39999E-02	9.39999E-02	
NUSF	3	.	.	0.0	0.0	
SCAPT	3	.	.	1.74830E-02	1.17495E-02	0.67205
SFISS	3	.	.	0.0	0.0	
SREM	3	.	.	2.03071E-02	1.42007E-02	
STR	3	.	.	1.72622E-01	1.59994E-01	
SMTOT	3	IN	3	1.62470E-01	1.47208E-01	
SMTOT	3	IN	4	2.82415E-03	2.45129E-03	
CHI	4	.	.	1.00000E-03	1.00000E-03	
NUSF	4	.	.	0.0	0.0	
SCAPT	4	.	.	4.34512E-02	3.47514E-02	0.79978
SFISS	4	.	.	0.0	0.0	
SREM	4	.	.	4.34511E-02	3.47513E-02	
STR	4	.	.	2.78651E-01	2.68420E-01	
SMTOT	4	IN	4	2.75782E-01	2.66896E-01	

with: CHI = group averaged fission spectrum
 SCAPT = capture cross section
 SFISS = fission cross section
 NUSF = SFISS * average number of fission neutrons
 SREM = removal cross section (absorption and downscattering)
 STR = transport cross section
 SMTOT = scattering cross section (no upscattering)

Table 6

SAC reactivity worths measured and calculated with the new method at (a) critical, (b) full SCP insertion depth; the effective absorber concentrations are 62 % / 48 % for the lower/upper SAC.

	$\Delta\rho_{\text{meas}}$ (pcm)	$\Delta\rho_{\text{calc}}$ (pcm)	$\Delta\rho_{\text{calc}}/\Delta\rho_{\text{meas}}$
(a)	1039	1049	1.01
(b)	1191	1164	0.98

Table 7

Results of transport calculations for a core cylinder, sodium follower, and SACs from different calculational models (RZ and R θ geometry) as described in section 5. Given are the used bucklings B_F^2 and B_S^2 , the multiplication constants and corresponding reactivity differences, energy group summed fluxes ϕ_S and ϕ_F , averaged over singularity and fuel regions, and their ratio. The last entry of the table, denoted "ref.", refers to calculations with the reference transport model (cf. Fig. 3), however with different bucklings for the singularity and fuel regions (26 energy groups, GRUCAL cross sections).

		B_F^2	B_S^2	k-eff	ρ_{Na-P}	ϕ_S	ϕ_F	ϕ_S/ϕ_F
		$(10^{-4}cm^{-2})$			(pcm)			
RZ, $H_c=100$ cm	Fuel			0.972832				
	Na-Follower			0.966081		5.9009-5	3.1190-5	1.8919
	Lower SAC			0.953108	1408.9	3.0042-5	3.0796-5	0.9755
	Upper SAC			0.949649	1791.1	2.2394-5	3.0675-5	0.7300
R θ	Fuel	8.36	-	0.972816				
	Na-Follower	8.36	5.57	0.966073		2.3552-2	1.2479-2	1.8873
R θ , ring	Lower SAC	8.36	4.54	0.953127	1405.9	1.2002-2	1.2323-2	0.9739
	Upper SAC	8.36	4.54	0.949630	1792.3	8.9339-3	1.2274-2	0.7279
R θ , "ref."	Lower SAC	8.36	4.54	0.953041	1415.4			
	Upper SAC	8.36	4.54	0.949362	1822.0			

Table 8

Results of transport calculations for a core cylinder and sodium follower in R θ geometry with material-independent buckling as described in section 5. The follower and sheath regions are described in different ways, and the buckling correction is derived from different types of transport cross sections. Given are the multiplication constants and corresponding reactivity differences (26 energy groups, $B^2=8.36 \times 10^{-4} \text{ cm}^{-2}$).

	treatment of Na and sheath regions	DB ² derived with	k-eff	$\rho_{\text{fuel}}-\rho_{\text{Na}}$ (pcm)
Fuel	-	GRUCAL- Σ_{tr}	0.972816	
Na-Follower	separate	GRUCAL- Σ_{tr}	0.964287	909.1
	homogenized	GRUCAL- Σ_{tr}	0.965385	791.2
	separate	KAPER4- $\Sigma_{\text{tr,ax}}$	0.966185	705.4
	homogenized	KAPER4- $\Sigma_{\text{tr,ax}}$	0.966125	711.8
	homogenized	KAPER4- Σ_{tr}	0.966194	704.5

Table 9

SAC reactivity worths measured and calculated with the improved new method (see section 5) at (a) critical, (b) full SCP insertion depth; the effective absorber concentrations are 75 % / 62 % for the lower/upper SAC.

	$\Delta\rho_{\text{meas}}$ (pcm)	$\Delta\rho_{\text{calc}}$ (pcm)	$\Delta\rho_{\text{calc}}/\Delta\rho_{\text{meas}}$
(a)	1039	1148	1.10
(b)	1191	1268	1.06

FIGURE CAPTIONS

Fig. 1. (a) Horizontal cuts through the lower and upper parts of a SPX-1 complementary shut-down system rod SAC. (b) Sketch of the axial structure of the SAC. Lengths are given in mm.

Fig. 2. Models of both SAC parts used for the old KAPER4 analysis. Lengths are given in mm.

Fig. 3. (a) Models of both SAC parts used for the transport reference calculations. Lengths are given in mm, angles in radians. It should be noted that the explicit models used here and the associated cylindrical models of the present cross section production (Fig. 9) used a cylindricalized outer subassembly diameter (90.83 mm) that differed somewhat from the one used in the former analysis (94.23 mm). While the latter was derived on the basis of the reactor pitch at 180°C (179.482 mm), the present work was simply based on the flat-to-flat dimension at 20°C: 173.0 mm. This simplification is not considered to have a significant influence on the results of the present study. (b) Detailed sketch of the upper SAC with notations used in the text.

Fig. 4. Contour plots of the lower SAC neutron fluxes for one quadrant of the model of Fig. 3a, calculated with four-group transport theory. Numerical values of contour levels are given in units of 10^{-3} cm^{-2} .

Fig. 5. Radial dependence of the lower SAC neutron fluxes for the model of Fig. 3a, calculated with four-group transport theory and corresponding diffusion approximation.

Fig. 6. Radial dependence of follower and SAC neutron fluxes for the model of Fig. 3a, calculated with four-group transport theory.

Fig. 7. Models of both SAC parts with a refined description of the absorber pins, used for supplementary transport calculations.

Fig. 8. Contour plots of the lower SAC neutron fluxes for one quadrant of the model of Fig. 7a, calculated with four-group transport theory. Numerical values of contour levels are given in units of 10^{-3} cm^{-2} , and are consistent with those of Fig. 4.

Fig. 9. Models of both SAC parts used for the new KAPER4 calculations for producing homogeneous macroscopic cross sections. Lengths are given in mm.

Fig. 10. Reactivity differences between sodium follower and SACs for the homogeneous diffusion model as a function of the boron carbide content of the SAC, calculated with diffusion approximation.

Fig. 11. Variation of the reactivity differences between sodium follower and SACs with varying boron carbide concentration at critical SCP insertion depth from two-dimensional whole core diffusion calculations.

Fig. 1: CONTROL ROD GEOMETRY

Lower SAC

Upper SAC

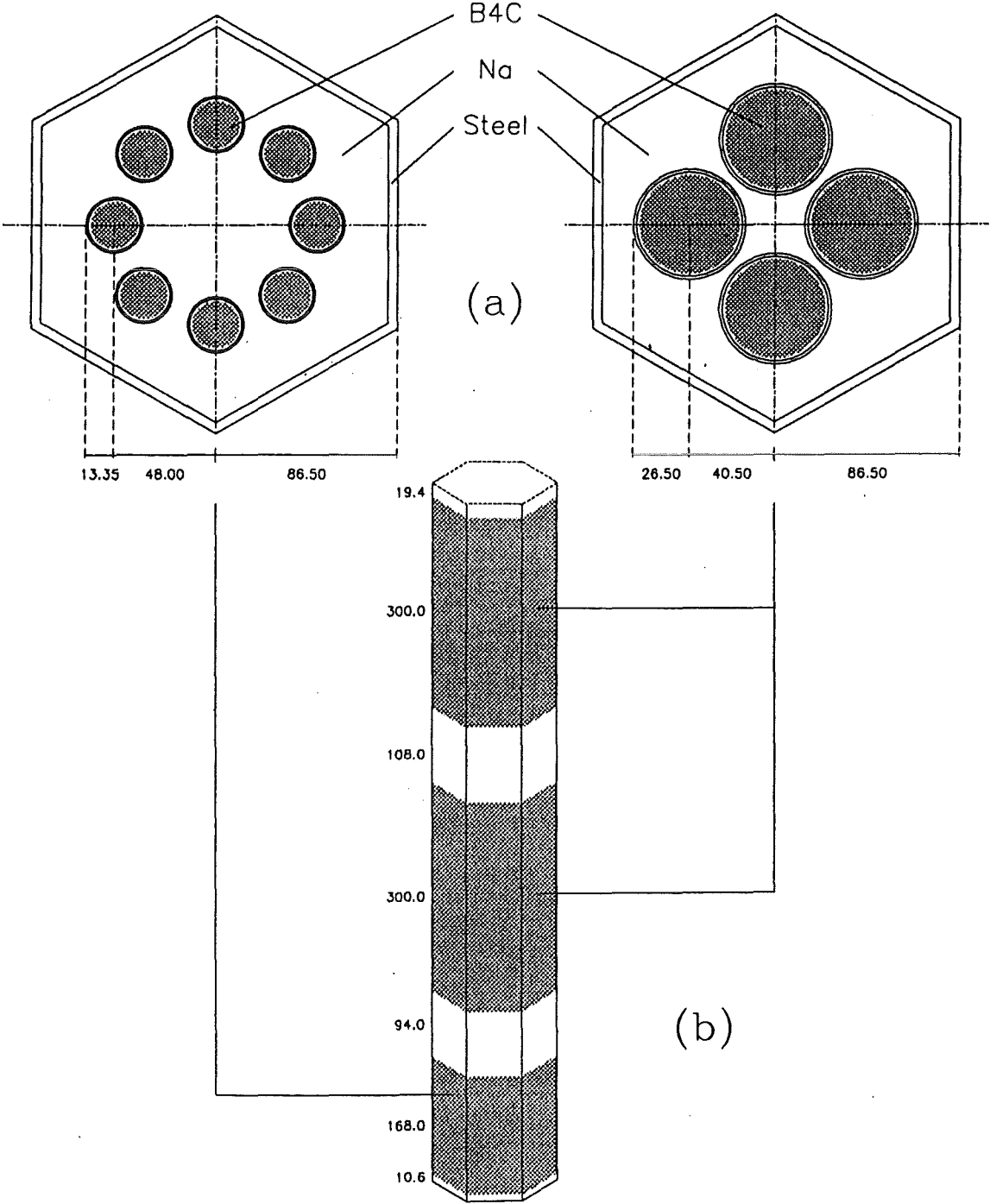


Fig. 2: OLD SUPERCELL MODEL

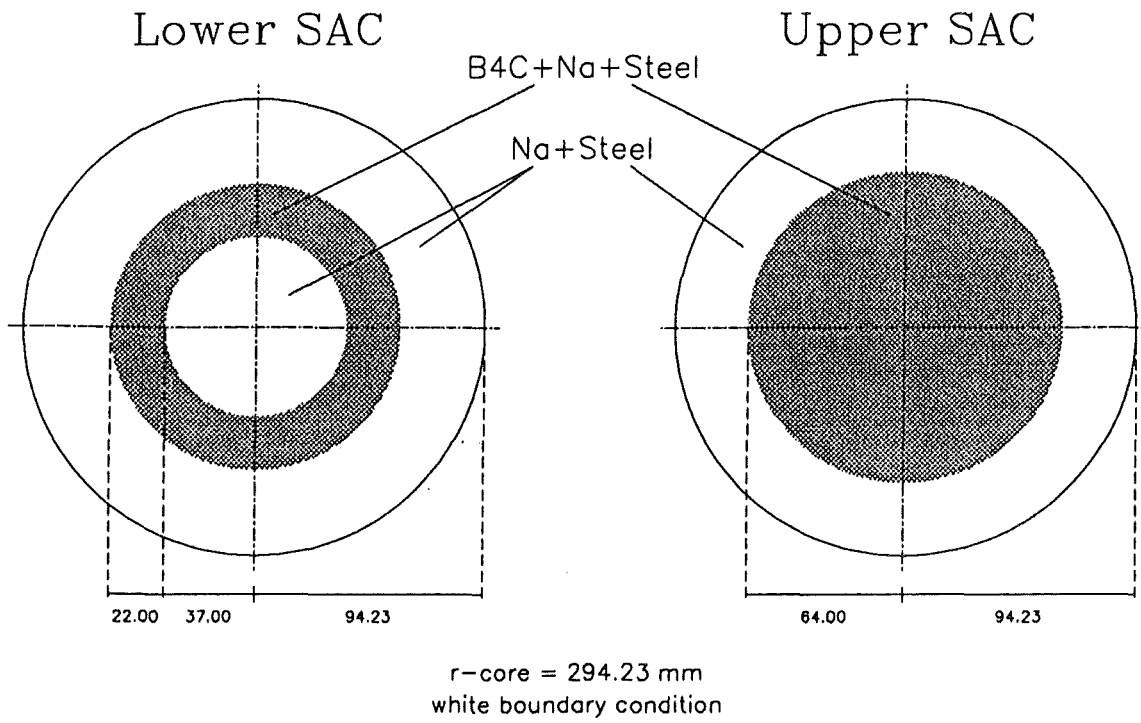


Fig. 3: REFERENCE TRANSPORT MODEL

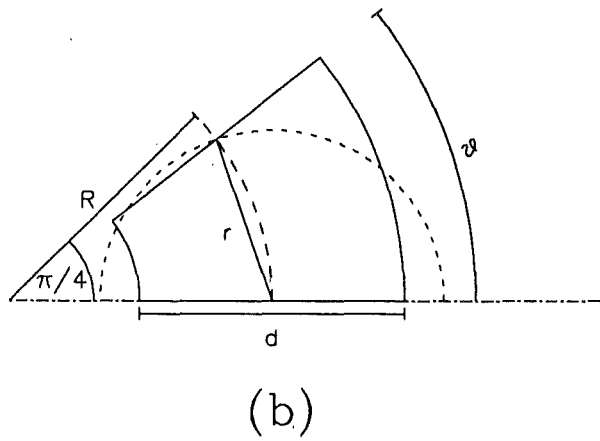
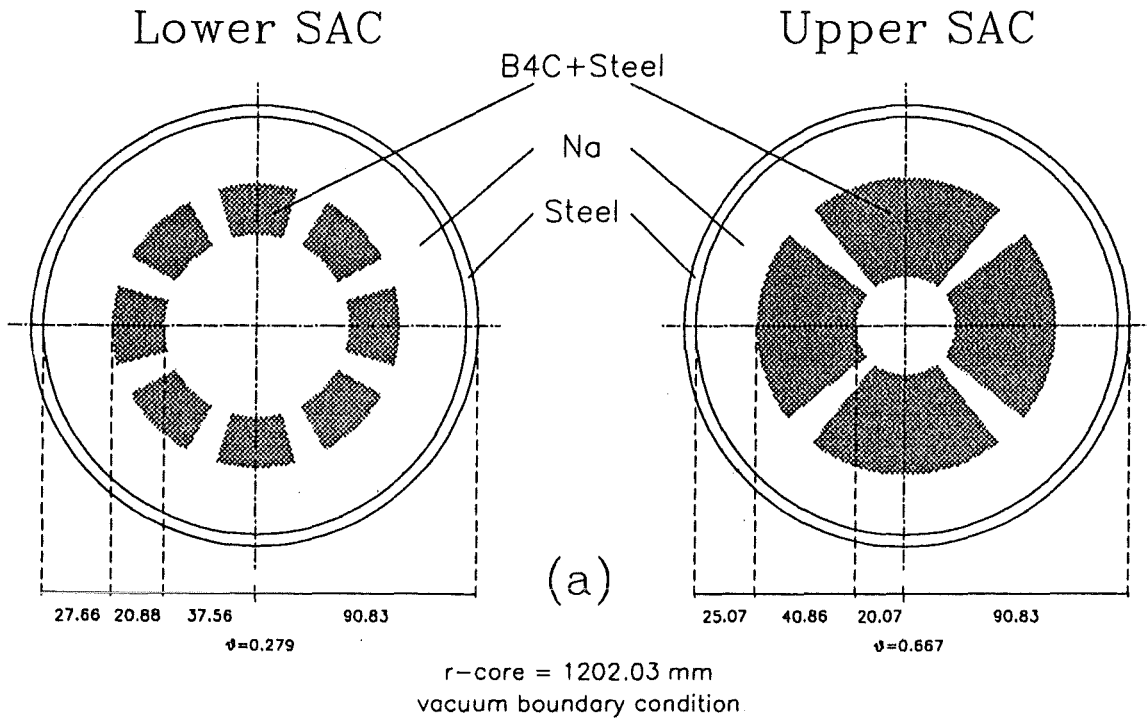
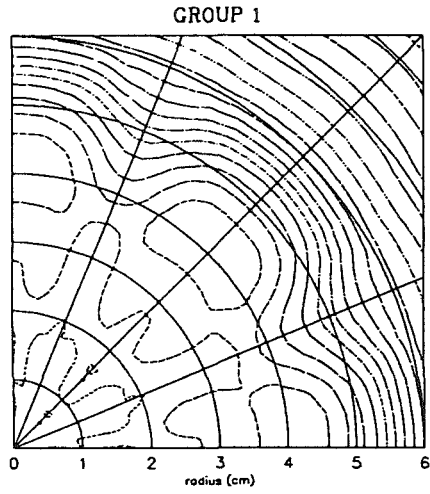
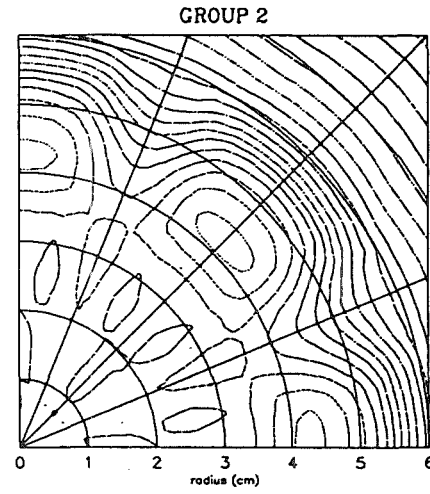


Fig. 4: LOWER SAC, 4 GROUPS, TRANSPORT



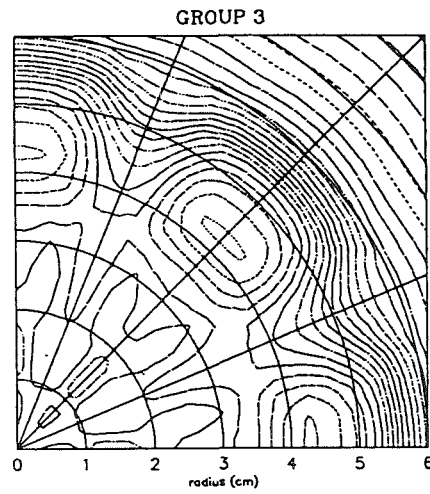
flux (10⁻³ cm⁻²)

.....	0.916
.....	0.926
.....	0.936
.....	0.946
.....	0.956
.....	0.966
.....	0.976
.....	0.986
.....	0.996
.....	1.006
.....	1.016
.....	1.026
.....	1.036
.....	1.046
.....	1.056
.....	1.066
.....	1.076
.....	1.086
.....	1.096



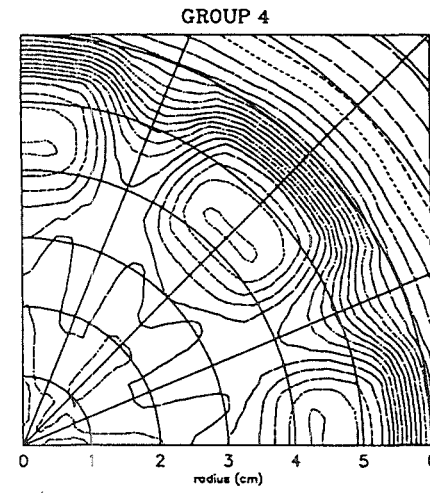
flux (10⁻³ cm⁻²)

.....	2.13
.....	2.18
.....	2.21
.....	2.24
.....	2.27
.....	2.3
.....	2.33
.....	2.36
.....	2.39
.....	2.42
.....	2.45
.....	2.48
.....	2.51
.....	2.54
.....	2.57
.....	2.6
.....	2.63
.....	2.66
.....	2.69



flux (10⁻³ cm⁻²)

.....	5.04
.....	5.14
.....	5.24
.....	5.34
.....	5.44
.....	5.54
.....	5.64
.....	5.74
.....	5.84
.....	5.94
.....	6.04
.....	6.14
.....	6.24
.....	6.34
.....	6.44
.....	6.54
.....	6.64
.....	6.74
.....	6.84
.....	6.94
.....	7.04
.....	7.14
.....	7.24
.....	7.34



flux (10⁻³ cm⁻²)

.....	0.32
.....	0.37
.....	0.42
.....	0.47
.....	0.52
.....	0.57
.....	0.62
.....	0.67
.....	0.72
.....	0.77
.....	0.82
.....	0.87
.....	0.92
.....	0.97
.....	1.02
.....	1.07
.....	1.12
.....	1.17
.....	1.22
.....	1.27
.....	1.32
.....	1.37
.....	1.42
.....	1.47

Fig. 5: LOWER SAC, 4 GROUPS, TRANSPORT & DIFFUSION

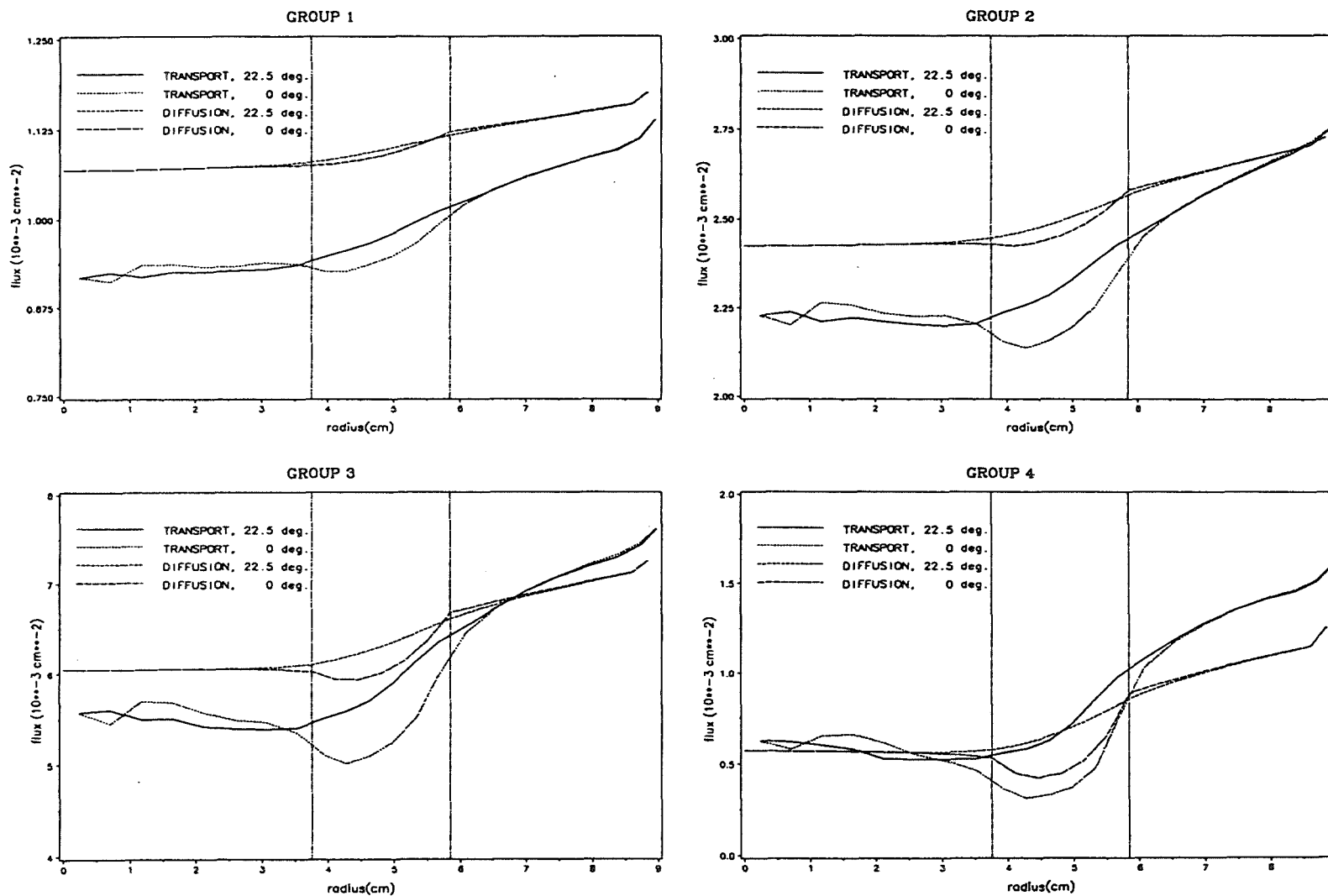


Fig. 6: 4 GROUPS, TRANSPORT

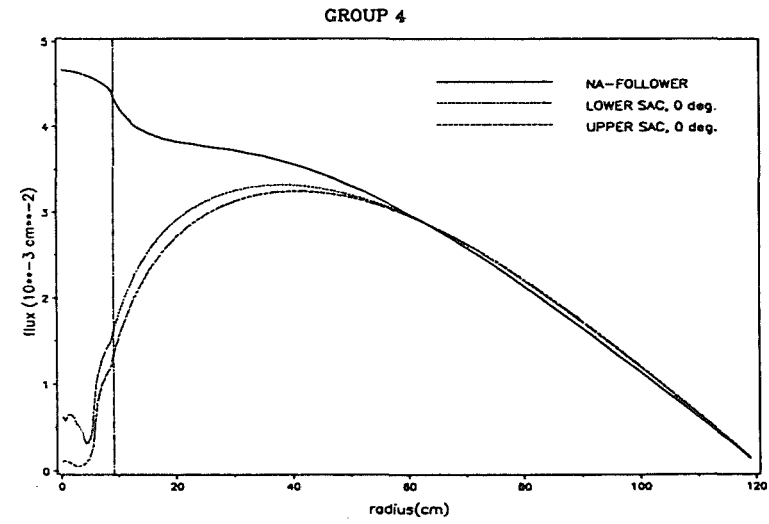
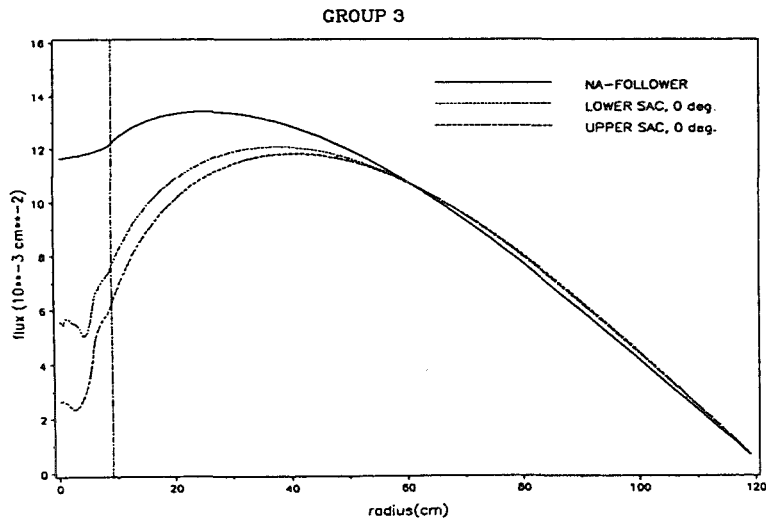
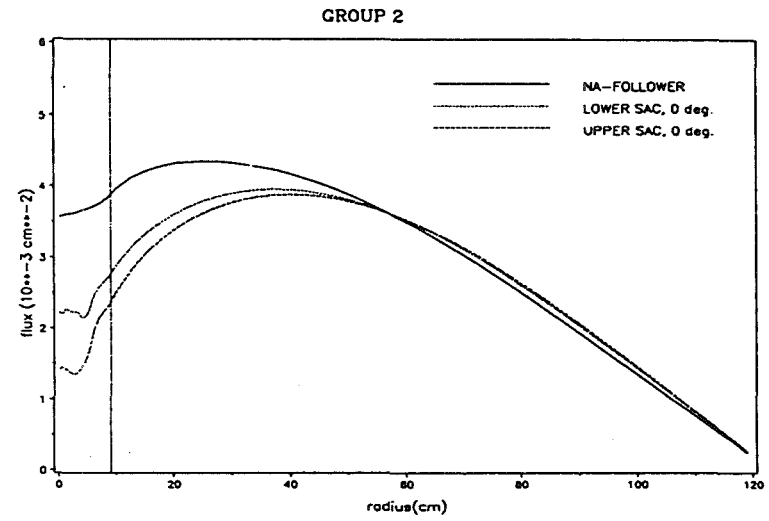
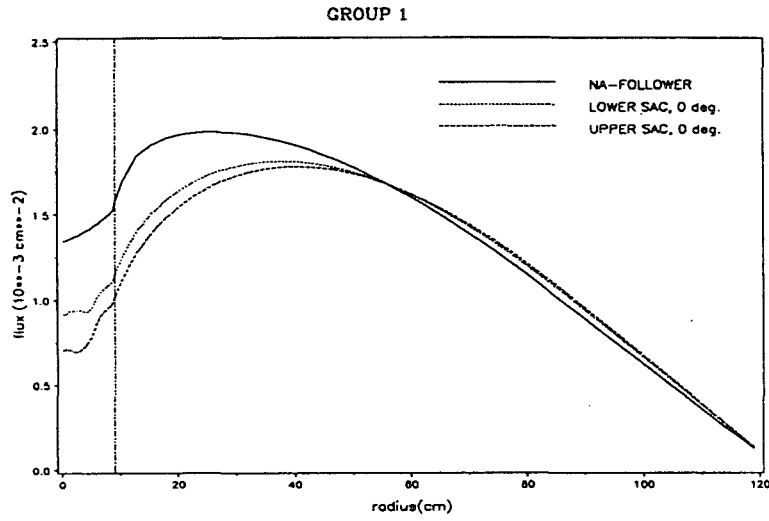


Fig. 7: REFINED TRANSPORT MODEL

Lower SAC

Upper SAC

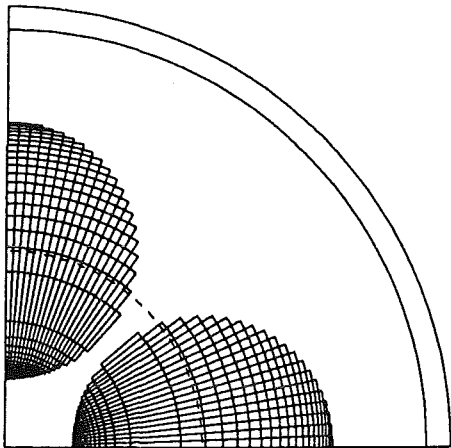
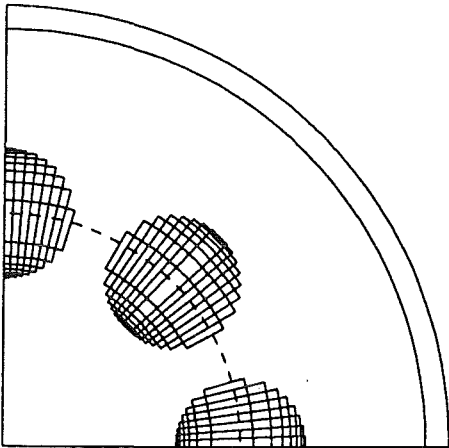
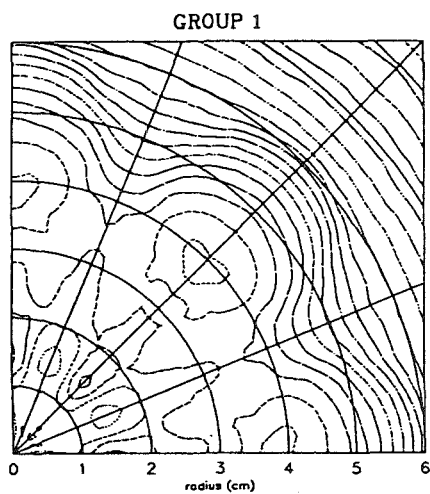
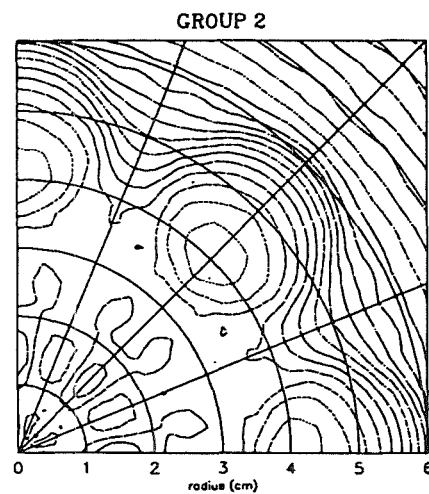


Fig. 8: LOWER SAC (DETAILED REPRESENTATION), 4 GROUPS, TRANSPORT



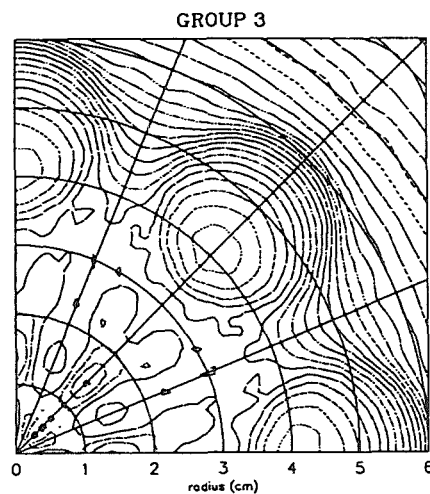
flux (10^{-3} cm^{-2})

0.918
0.928
0.938
0.948
0.955
0.966
0.976
0.986
0.996
1.006
1.018
1.028
1.038
1.046
1.056
1.066
1.076
1.086
1.096



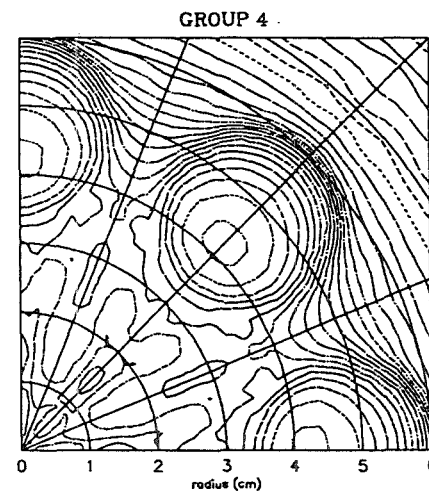
flux (10^{-3} cm^{-2})

2.15
2.18
2.21
2.24
2.27
2.3
2.33
2.36
2.39
2.42
2.45
2.48
2.51
2.54
2.57
2.6
2.63
2.66
2.68



flux (10^{-3} cm^{-2})

5.04
5.14
5.24
5.34
5.44
5.54
5.64
5.74
5.84
5.94
6.04
6.14
6.24
6.34
6.44
6.54
6.64
6.74
6.84
6.94
7.04
7.14
7.24
7.34



flux (10^{-3} cm^{-2})

0.32
0.37
0.42
0.47
0.52
0.57
0.62
0.67
0.72
0.77
0.82
0.87
0.92
0.97
1.02
1.07
1.12
1.17
1.22
1.27
1.32
1.37
1.42
1.47

Fig. 9: NEW SUPERCELL MODEL

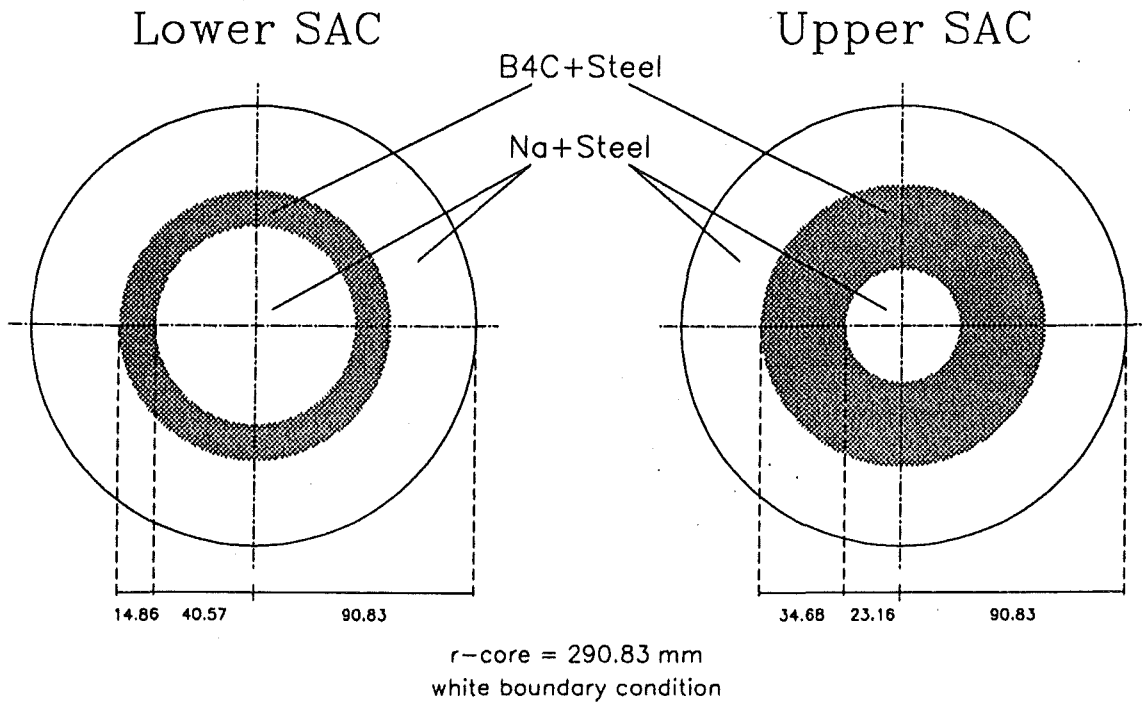


Fig. 10: ROD WORTHS IN THE HOMOGENEOUS DIFFUSION MODEL

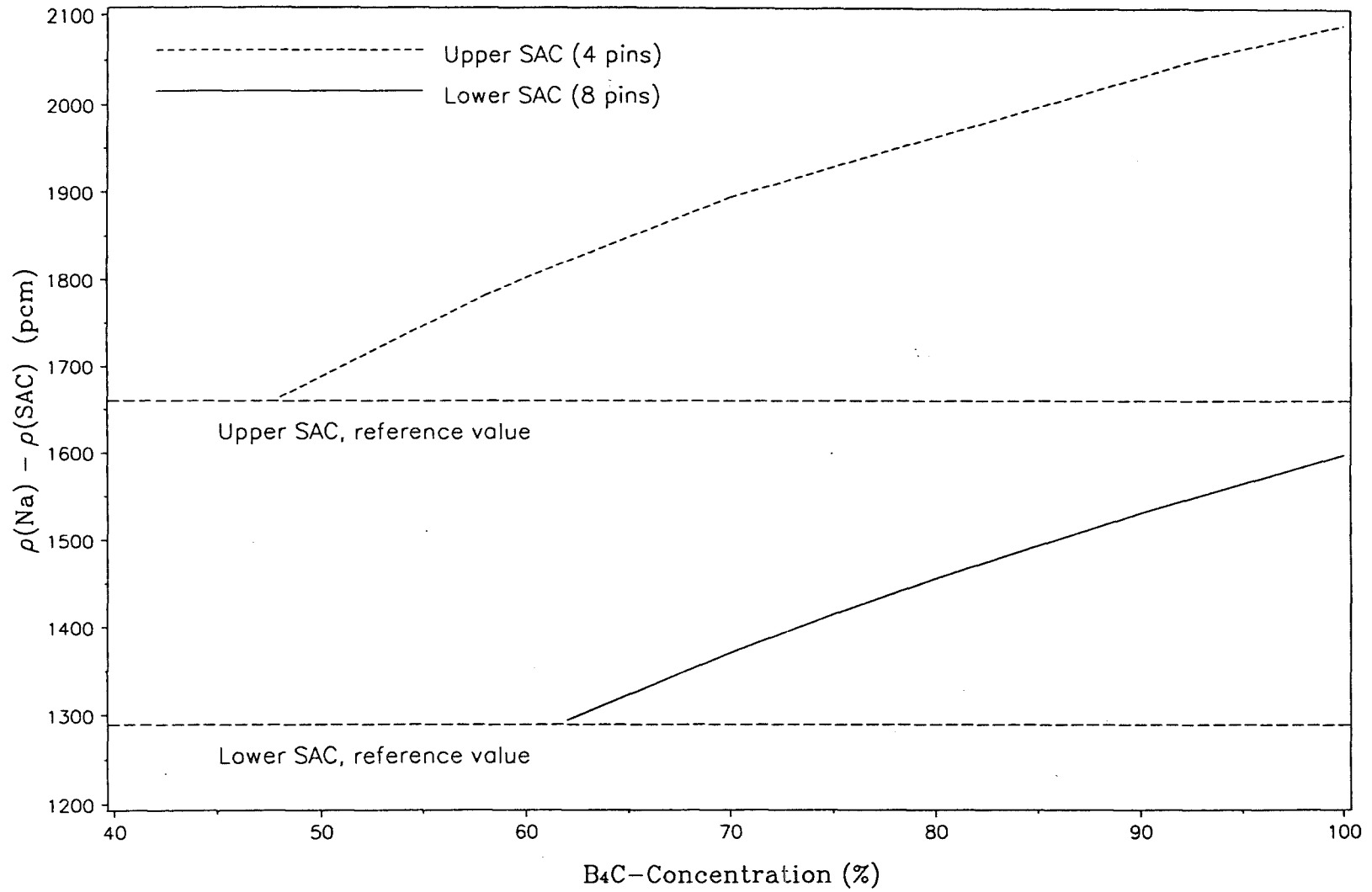


Fig. 11: 2-D WHOLE CORE DIFFUSION CALCULATION

